Economic Geology, v. 109, pp. 1763–1785

SCIENTIFIC COMMUNICATIONS

*CONTRASTING PARENTAL MAGMA COMPOSITIONS FOR THE HONGGE AND PANZHIHUA MAGMATIC Fe-Ti-V OXIDE DEPOSITS, EMEISHAN LARGE IGNEOUS PROVINCE, SW CHINA**

Zhong-Jie Bai,[1] Hong Zhong,[1,†] Chusi Li,[2] Wei-Guang Zhu,[1] De-Feng He,[1] and Liang Qi[1]

[1] *State Key Laboratory of Ore Deposit Geochemistry, Institute of Geochemistry, Chinese Academy of Sciences, Guiyang 550002, China*

[2] *Department of Geological Sciences, Indiana University, Bloomington, Indiana 47405*

Abstract

Many ~260 Ma mafic-ultramafic layered intrusions, including Hongge and Panzhihua, in the Emeishan large igneous province, southwestern China host world-class Fe-Ti-V oxide ore deposits. These two most important ore-bearing intrusions show differences in lithology and mineral chemistry. The most important orebodies in the Hongge intrusion occur as concordant layers in the middle part of the intrusion, closely associated with clinopyroxenites. Titanomagnetite and Mg-rich ilmenite are the major ore minerals of the Hongge deposit. Coexisting clinopyroxene contains >1.7 wt % TiO_2. These data indicate high Ti parental magma for the Hongge ore-bearing clinopyroxenites. In the Panzhihua intrusion, the most important orebodies also occur as concordant layers but in its lower part instead of middle part. In contrast with the Hongge deposit, the most important host rocks of the Panzhihua deposit are gabbros, not clinopyroxenites. In addition, ilmenite is rare and titanomagnetite is predominant in the Panzhihua deposit. Coexisting clinopyroxene in the Panzhihua deposit contains <1.6 wt % TiO_2. The contrasting lithologic and mineral compositions indicate that the parental magma for the Hongge deposit has higher TiO_2 than that for the Panzhihua deposit. The compositions of clinopyroxene from the Panzhihua and Hongge deposits indicate that their parental magmas are also different in MgO/FeO and trace element ratios as well. Calculations using average experimental Mg-Fe exchange coefficient and trace element partition coefficients between clinopyroxene and magma show that the Hongge parental magma has higher MgO/FeO ratios and more fractionated mantle-normalized trace element patterns than the Panzhihua parental magma. The estimated compositions of the parental magmas for the Hongge and Panzhihua ore-bearing lithologies resemble the average compositions of the Longzhoushan-type high Ti basalts and Ertan-type intermediate Ti basalts in the Emeishan large igneous province, respectively. The new trace element data from this study, together with available Sr-Nd isotope data for the ore-bearing intrusions from literature, support a new petrogenetic model involving selective assimilation of newly subducted, stagnant oceanic gabbroic slab above the deep-seated Emeishan mantle plume. This process and subsequent contamination with the upper crust played an important role in the variation of parental magma compositions between the Hongge and Panzhihua magmatic oxide ore deposits. Abundant Fe-Ti oxide ore deposits associated with less evolved basaltic magma in the Emeishan large igneous province than elsewhere in the world are attributed to selective assimilation of newly subducted, stagnant oceanic lithospheric slab by the ascending mantle plume-derived picritic magma that was originally undersaturated with Fe-Ti oxides.

Introduction

Several ~260 Ma mafic-ultramafic intrusions, such as Panzhihua, Hongge, Baima, and Taihe, in the Emeishan large igneous province, southwestern China, host world-class Fe-Ti-V oxide ore deposits (Fig. 1). Massive oxide ore layers (up to ~60 m thick in the Panzhihua, and ~84 and ~70 m thick in the Hongge and Baima intrusions, respectively; Zhong et al., 2002, 2005; Pang et al., 2009, 2010) occur in the lower or middle parts of the intrusions. The origins of oxide ores in these intrusions are hotly debated. Zhou et al. (2005, 2013) and Dong et al. (2013) proposed that the oxide ores formed by silicate-oxide liquid immiscibility while other researchers (e.g., Zhong et al., 2003, 2005; Ganino et al., 2008; Pang et al., 2008a, b, 2009, 2010; Wang et al., 2008; Zhang et al., 2008; Bai et al., 2012a, b; Hou et al., 2012; Shellnutt and Pang, 2012; Song et al., 2013; Luan et al., 2014) suggested they formed by accumulation of Fe-Ti oxides crystallized from Fe-Ti-rich basaltic magma. Regardless of mechanism, the variations of parental magma compositions for these deposits are poorly constrained. Many researchers (Zhong et al., 2005; Pang et al., 2008a, 2009, 2010; Wang et al., 2008; Zhang et al., 2008; Bai et al., 2012a, b; Hou et al., 2012; Shellnutt and Pang, 2012; Song et al., 2013; Luan et al., 2014) believe that the parental magmas for all of the ore-bearing intrusions in the Emeishan large igneous province are comparable to the coeval high-Ti basalts (TiO_2>2.5%, Ti/Y>500, Xu et al., 2001). However, these intrusions show different lithological and mineralogical controls on the occurrence of oxide ore horizons. For example, the most important orebodies in the Hongge intrusion are composed of titanomagnetite and Mg-rich ilmenite in the middle part of the intrusion, closely associated with clinopyroxenites (Zhong et al., 2002; Pang et al., 2008a; Bai et al., 2012b). In contrast, the most important orebodies in the Panzhihua intrusion are present in the lower part of the intrusion. The host rocks in Panzhihua deposit are dominated by gabbros instead of clinopyroxenites. Another difference between the Panhihua and

† Corresponding author: e-mail, zhonghong@vip.gyig.ac.cn

*A digital supplement to this paper is available at http://economicgeology.org/ and at http://econgeol.geoscienceworld.org/.

Submitted: July 29, 2013
Accepted: January 3, 2014

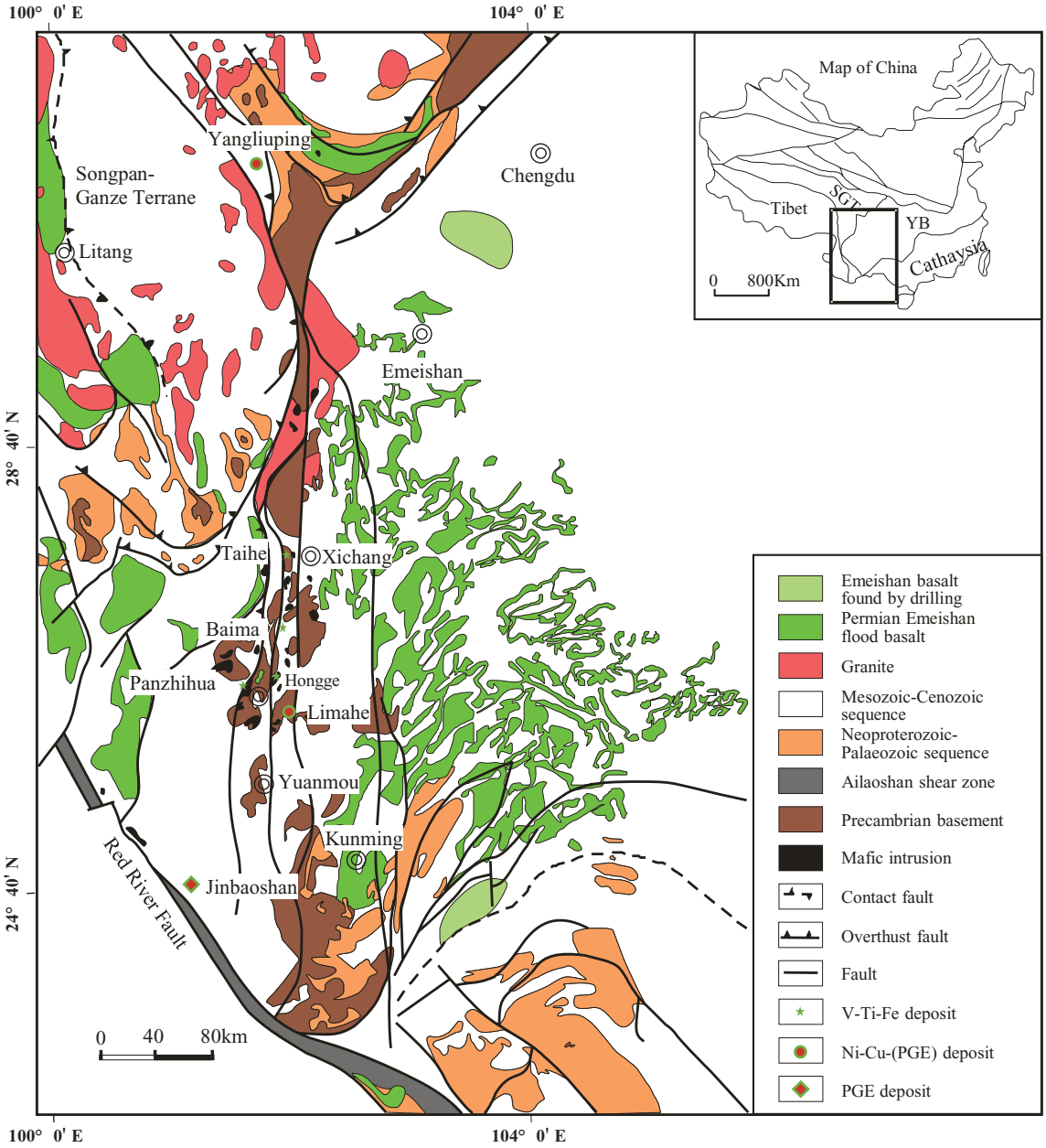

FIG. 1. Distribution of the Emeishan continental flood basalt province and contemporaneous mafic-ultramafic intrusions in southwestern China (modified from Zhou et al. 2002). SGT = Songpan-Ganze terrane; YB = Yangtze block.

Hongge deposits is that ilmenite is rare and titanomagnetite is predominant in the former (Pang et al., 2008a, b). Furthermore, the compositions of the coeval high-Ti basalts are highly variable in both major elements, trace elements and isotopes (Xu et al., 2001, 2007; Xiao et al., 2004; Zhang et al., 2006, 2009; Wang et al., 2007; Fan et al., 2008; Song et al., 2008; He et al., 2010; Hou et al., 2011a). The compositional variations in the coeval ore-bearing intrusions and coeval basalts may be related to similar petrologic processes. In the study we evaluate such a possibility as well as the controls on the compositional variations of parental magmas for the Hongge and Panzhihua deposits, using newly acquired mineralogical and petrological data.

Geologic Background

Regional geology

Southwestern China comprises the Yangtze Block to the east and the Tibetan Plateau to the west (Fig. 1). The basement of the Yangtze Block in this region is composed of Paleoproterozoic to Mesoproterozoic Huili Group or Kunyang Group low-grade metasedimentary and metavolcanic rocks, and Neoproterozoic metamorphic rocks of amphibolite to granulite facies (the Kangding Complex). In the larger Emeishan region the Yangtze basement is overlain by a thick sequence of Neoproterozoic metasedimentary rocks which in turn are overlain by Paleozoic carbonates and then by Permian continental

flood basalts. Triassic continental and marine sedimentary rocks and Jurassic-Cretaceous continental sediments are present locally. Rodinian (830–740 Ma) intrusive and extrusive rocks with compositions varying from ultramafic to felsic have been found in the western margin of the Yangtze block (e.g., Li et al., 2003, 2006; Zhou et al., 2006; Zhu et al., 2006).

The Emeishan large igneous province and associated Fe-Ti-V oxide ore deposits

The distribution and compositional variations of the Emeishan large igneous province have been described in many previous studies (e.g., Chung and Jahn, 1995; Xu et al., 2001, 2007; Xiao et al., 2004; Zhang et al., 2006, 2008). A brief summary based on the previous studies is given below. The Emeishan large igneous province is composed of picrites, flood basalts, rhyolitic/trachytic flows, mafic–ultramafic layered intrusions, granites, and syenites. The volcanic sequence covers an area exceeding 5×10^5 km^2. The thickness of the volcanic sequence varies from several hundred meters in the eastern part to >5,000 m in the western part. Both tholeiitic and alkaline basalts are present in the volcanic sequence. They have been divided into high Ti (TiO_2 >2.5 wt %, Ti/Y >500) and low Ti (TiO_2 <2.5 wt %, Ti/Y <500) basalts by some researchers (Xu et al., 2001; Xiao et al., 2004). Other researchers have questioned the usefulness of such classification for the Emeishan flood basalts (Hanski et al., 2010; He et al., 2010; Hou et al., 2011a; Kamenetsky et al., 2012, Li et al., 2012). He et al. (2010) pointed out that part of the Emeishan basalts with intermediate TiO_2 contents (e.g., TiO_2 = 2–3.5 wt % in whole rock) are close to the boundary of low and high Ti series. Such basalts intermediate between the high and low Ti end members strongly suggest a compositional continuum in TiO_2 over significant ranges of MgO (Kamenetsky et al., 2012). Common phenocrysts in the basalts and associated picrites are clinopyroxene plus plagioclase and olivine plus Cr spinel, respectively. The groundmass of these high to low Ti volcanic rocks are composed of small plagioclase and clinopyroxene crystals with diameter <100 μm and micro-Fe-Ti oxides with diameters <40 μm.

Some of the mafic-ultramafic layered intrusions in the Emeishan large igneous province host important Fe-Ti oxide ore deposits in their lower or middle parts. They are exposed along the N-S–trending major faults in the Panxi region due to significant uplift and erosion in this region (Fig. 2). The most important Fe-Ti oxide ore-bearing intrusions in the region are the Hongge (Fig. 3), Panzhihua (Fig. 4), Xinjie, Baima, and

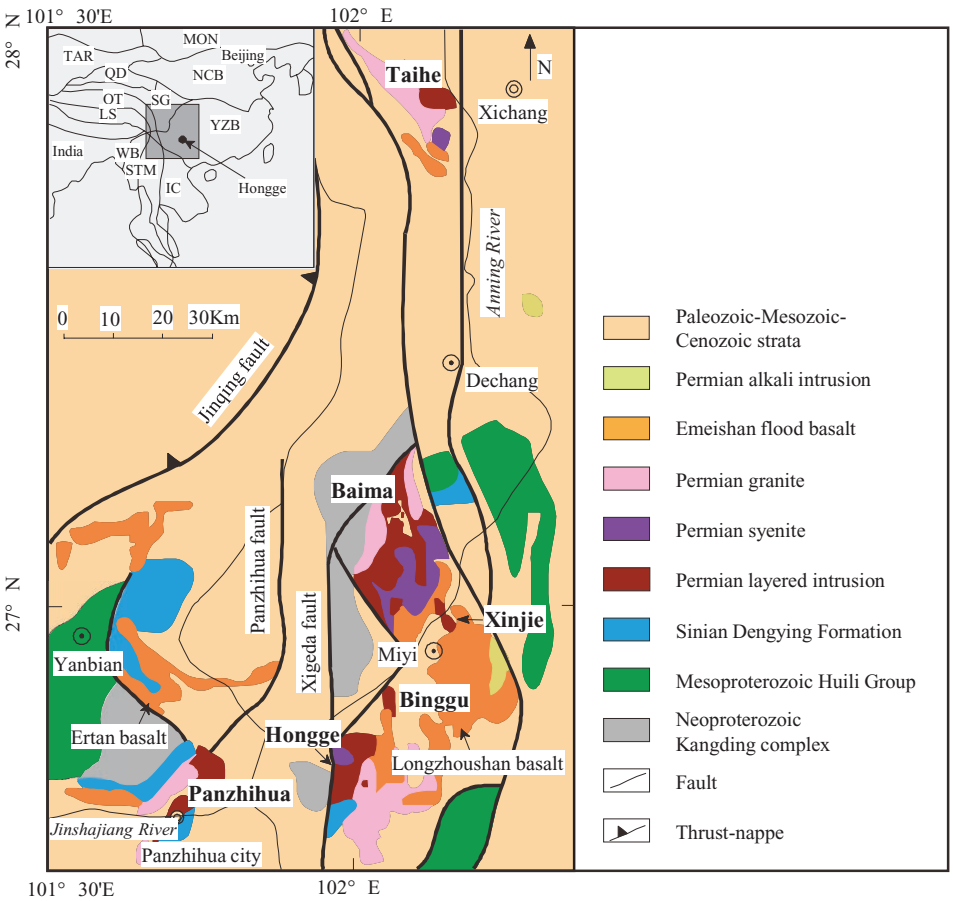

FIG. 2. Regional geologic map of the Pan-Xi region, showing the locations of the mafic-ultramafic layered intrusions that host important Fe-Ti-V oxide ore deposits (modified after Liu et al. 1985, and Bai et al., 2012b). Inset shows major tectonic units in China and the study area (modified after Chung and Jahn, 1995). Abbreviations: HI = Himalayan, IC = Indochina, LS = Lhasa, MON = Mongolia, NCB = North China block, QD = Qaidam, QT = Qiangtang, SG = Songpan-Ganze accretionary complex, STM = Shan-Thai-Malay, TAR = Tarim, WB = West Burma, YZB = Yangtze block.

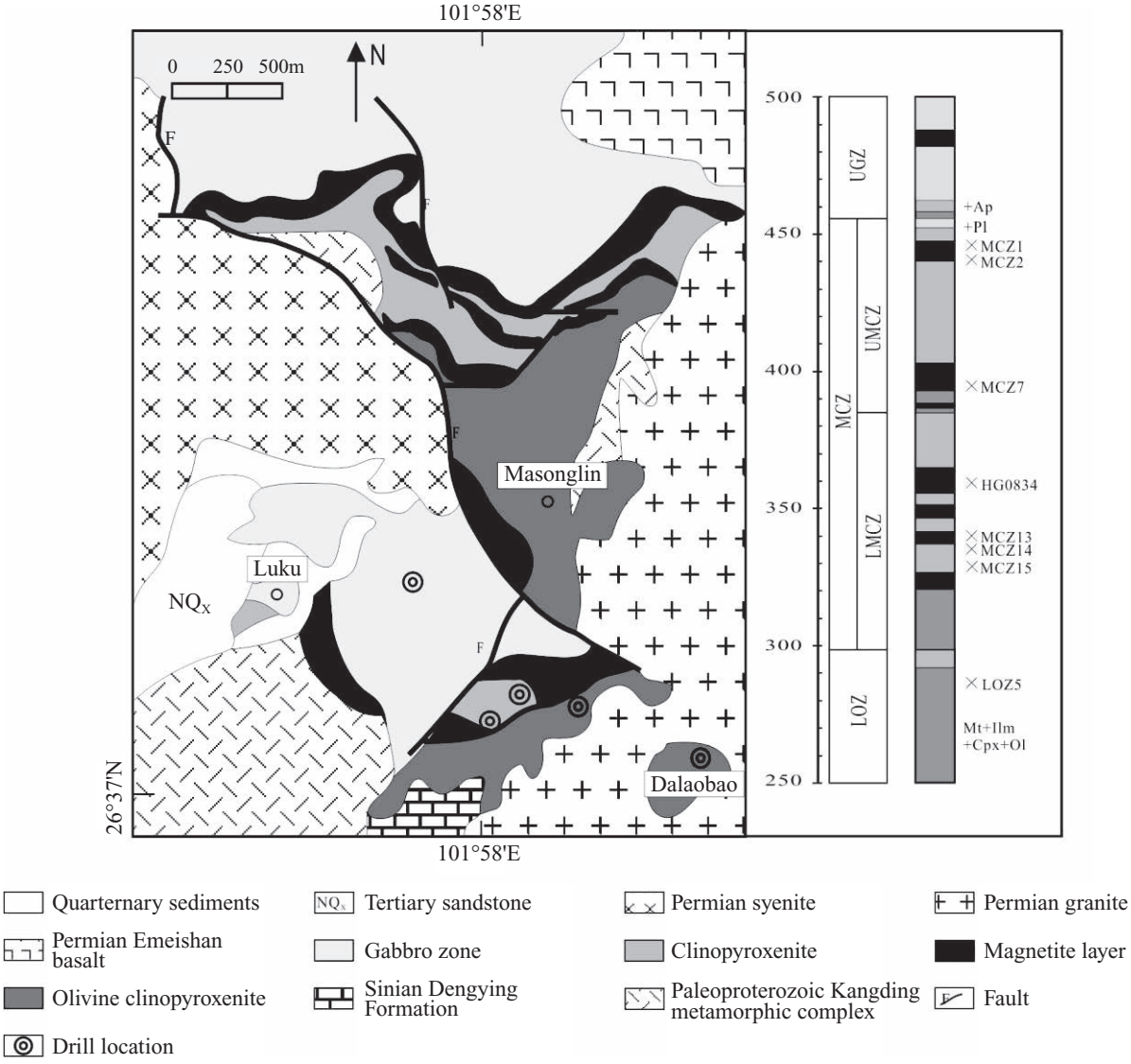

FIG. 3. Simplified geologic map of the Hongge intrusion (modified from Yao et al., 1993, and Bai et al., 2012b) and a composite stratigraphic column with sample locations. Abbreviations: LOZ = lower olivine clinopyroxenite zone, LMCZ = lower subzone of the middle clinopyroxenite zone, UGZ = upper gabbro zone, UMCZ = upper subzone of middle clinopyroxenite zone.

Taihe intrusions. These five intrusions together contain a total ore reserve of ~7,209 Mt Fe_2O_3, ~559 Mt TiO_2, and ~17.4 Mt V_2O_3 with grades of 27 wt % FeO, 10.6 wt % TiO_2, and 0.24 wt % V_2O_3 (Ma et al., 2003; Zhong et al., 2005). Recently, zircon U-Pb dating results reveal that the mafic-ultramafic intrusions have a crystallization age of ~260 Ma (263 ± 3 Ma for Panzhihua, 259.3 ± 1.3 Ma for Hongge, 259 ± 3 Ma for Xinjie; Zhou et al., 2002, 2005, 2008; Zhong and Zhu, 2006), which is similar to the zircon U-Pb age (259.6 ± 5.9 Ma) of the associated flood basalts in the region (Fan et al., 2004, 2008; Lai et al., 2012).

Lithology of the Hongge and Panzhihua Intrusions

Hongge intrusion

The 16-km-long, 3- to 6-km-wide, and 1.2-km-thick Hongge layered intrusion (Fig. 3) has a zircon U-Pb age of 259.3 ± 1.3 Ma (Zhong and Zhu, 2006). The geology of the Hongge intrusion has been described in details by Zhong et al. (2002, 2003), Bai et al. (2012a, b), and Wang et al. (2013). A brief description is given below. The Hongge intrusion intruded limestones of the Sinian Dengying Formation and granitic gneisses of the Neoproterozoic Kangding Complex. The limestones in direct contact with the intrusion were metamorphosed to marbles (PXGT, 1987). The northeastern part of the intrusion is covered by ~180-m-thick flood basalts. Late Permian alkaline granites and alkaline syenites cut across the northwestern contact zone between the Hongge intrusion and its country rocks. Based on cumulus mineral stratigraphy, the Hongge intrusion is divided into a lower olivine clinopyroxenite zone, a middle clinopyroxenite zone, and an upper gabbro zone (PXGT, 1987). The middle clinopyroxenite zone is further divided into two subzones, lower subzones of the middle clinopyroxenite zone at the bottom and upper subzones of the

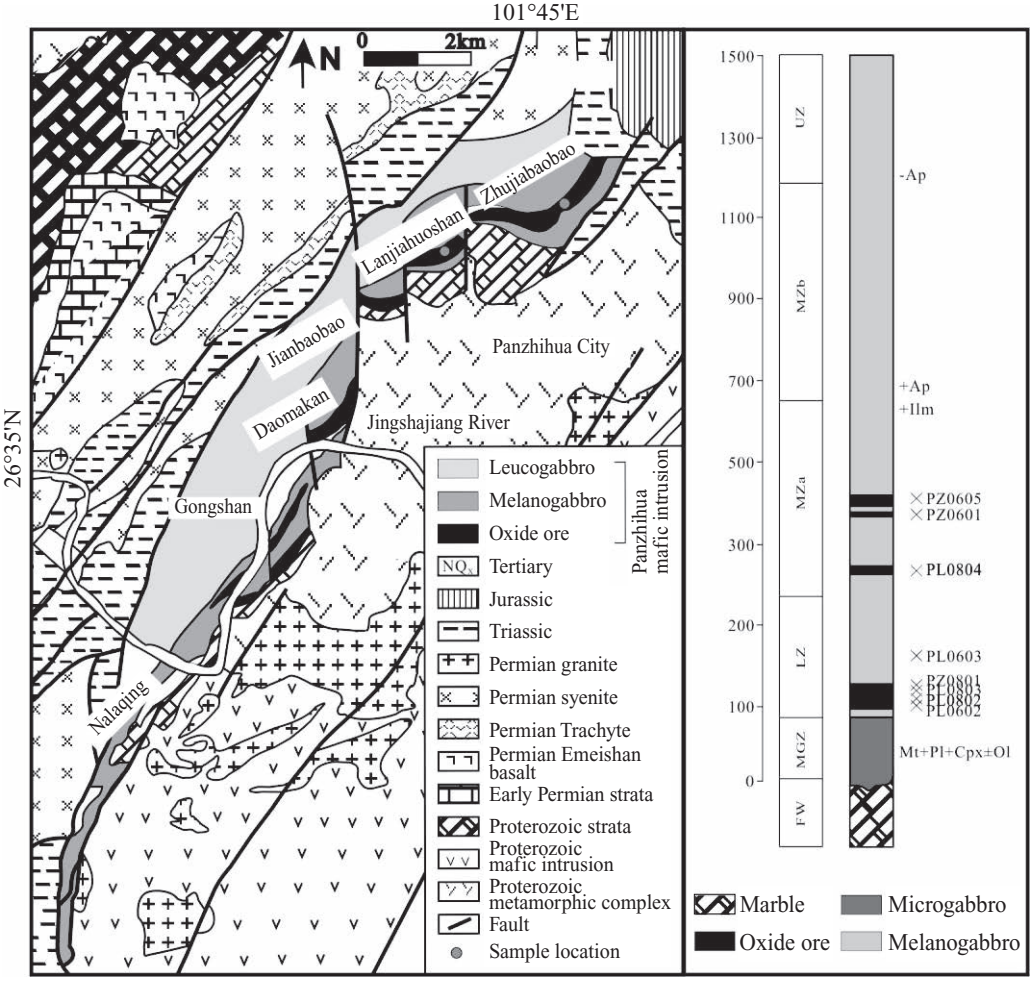

FIG. 4. Simplified geologic map of the Panzhihua intrusion (modified after Zhou et al., 2005) and a composite stratigraphic column (modified after Pang et al., 2009) with sample locations. Abbreviations: FW = footwall, MGZ = Marginal zone, LZ = Lower zone, MZa = Middle zone a; MZb = Middle zone b, UZ = Upper zone.

middle clinopyroxenite zone at the top (Zhong et al., 2002). The bases of the lower olivine clinopyroxenite zone and two subzones of the middle clinopyroxenite zone are marked by the appearance of olivine, whereas the base of the upper gabbro zone is marked by the appearance of abundant euhedral apatite. Fe-Ti oxide orebodies mainly occur in the lower and middle parts of the two subzones of the middle clinopyroxenite zone (Fig. 3) as concordant layers with variable thickness.

The lower olivine clinopyroxenite zone is ~340 m thick and composed mainly of ultramafic rocks. Olivine clinopyroxenite is predominant in the lower part of this zone. Minor clinopyroxenite is present in the upper part. In addition to olivine and clinopyroxene, the rocks also contain small amounts of interstitial amphibole and plagioclase. Olivine occurs as inclusions within clinopyroxene crystals as well as interlocking grains with clinopyroxene. The Fe-Ti oxides are composed of cumulus titanomagnetite and ilmenite, as euhedral to rounded grains between olivine and clinopyroxene or as inclusions or partial inclusions within the olivine and clinopyroxene. The total amounts of the Fe-Ti oxides are commonly less than 20 modal % in this zone and are thus subeconomic (Wang et al., 2013). The middle clinopyroxenite zone is ~150 m thick. It is composed of clinopyroxenite layers intercalated with concordant Fe-Ti oxide ore horizons. Some olivine and clinopyroxene crystals in this zone contain small rounded ilmenite and titanomagnetite inclusions (Fig. 5a, b). The modal proportion of the ilmenite inclusions is higher than that of the titanomagnetite inclusions. The total Fe-Ti oxides in this zone vary from less than 20 modal % in subeconomic ores to more than 85 modal % in massive ores. Both euhedral to rounded cumulus titanomagnetite and ilmenite crystals are present in all the rocks of the lower olivine clinopyroxenite zone and the middle clinopyroxenite zone (Fig. 5c). Generally, the proportions of ilmenite in the total Fe-Ti oxides increase with the decrease of total Fe-Ti oxides from about 15 to 20 modal % in massive ores to more than 50 modal % in subeconomic ores. The massive Fe-Ti-V oxide layers are up to 84 m thick and account for >70% of the Hongge Fe-Ti-V oxide ore deposit. Oxides in the massive ore samples are much coarser than in disseminated ores, closely packed, and commonly exhibit a dihedral angle close to 120° between grains (Bai et al., 2012b). There is about ~2,000 to 6,000 ppm V present in the titanomagnetite in this zone. The clinopyroxene in the middle clinopyroxenite zone commonly contains ilmenite exsolution lamellae [100] planes

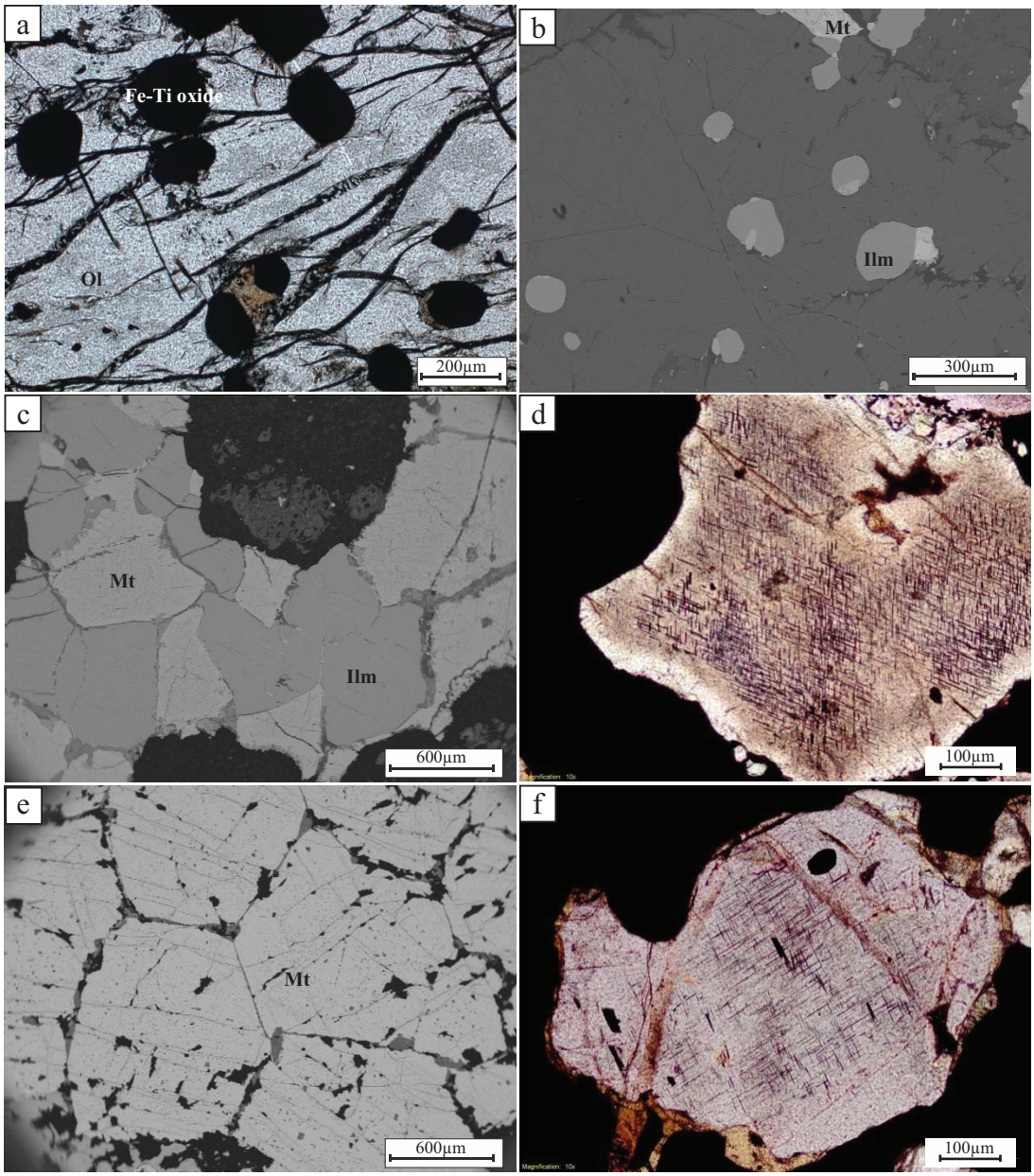

FIG. 5. Microphotographs and BSE images of Fe-Ti oxides from the Hongge and Panzhihua deposits. a, b. Small, rounded ilmenite and magnetite inclusions in olivine from the Hongge intrusion. c. Abundant ilmenite and magnetite cumulate assemblages in ore-rich olivine clinopyroxenite layers in the Hongge intrusion. d. Ilmenite exsolutions in clinopyroxene from the Hongge intrusion. e. Massive titanomagnetite ores from the Panzhihua deposit. f. Ilmenite exsolutions in clinopyroxene from the Panzhihua intrusion.

(Fig. 5d). The upper gabbro zone is ~780 m thick. Distinct, euhedral apatite up to 15% occurs as a cumulus phase from the bottom of this zone. Some plagioclase and olivine crystals contain small apatite inclusions. The amounts of Fe-Ti oxides in this zone mainly vary from 5 to 35% and locally increase to form economic ore layers. The modals of apatite are higher in olivine-, clinopyroxene-, and Fe-Ti oxides-rich rocks than those in leucogabbro.

These oxide layers and their host rocks in the lower olivine clinopyroxenite zone and the middle clinopyroxenite zone of the Hongge intrusion contain elevated Ni (~0.10 wt %), Co (~0.02 wt %), and Cu (~0.04 wt %) due to the presence of 0.5 to 3.5% disseminated sulfides (PXGT, 1987). Pyrrhotite is the major sulfide mineral, accounting for ~90% of the sulfide assemblages. Other minor sulfides include pentlandite, pyrite, chalcopyrite, and cubanite. The Hongge intrusion exhibits PGE-depleted patterns compared with the coeval Emeishan picritic lavas, indicating that the sulfides formed by second-stage sulfide liquid segregation from the PGE-depleted magma and that the oxidation state of the Hongge magmatic system was more reduced than QFM +1.5 (Bai et al., 2012a).

Panzhihua intrusion

The 19-km-long and 2-km-thick Panzhihua intrusion (Fig. 4) has a zircon U-Pb age of 263 ± 3 Ma (Zhou et al., 2005). The geology of the intrusion has been described in detail by Zhou et al. (2005) and Pang et al. (2008a, b, 2009) and important features are summarized here. The surface exposure covers an area of ~30 km^2. The immediate country rocks are almost exclusively the late Neopoterozoic dolomitic limestones of the Dengying Formation. The intrusion is divided into four zones: a Marginal zone, a Lower zone, a Middle zone, and an Upper zone. The Middle zone has been further divided in to subzones A (lower) and B. The ~40-m-thick Marginal zone is ~40 m thick and composed of hornblende-bearing microgabbro intercalated with olivine gabbro. Marble xenoliths are common in the lower part of this zone. In addition to olivine, clinopyroxene, and plagioclase, minor amounts of hornblende and Fe-Ti oxides are also present in this zone. The ~110-m-thick Lower zone is composed of alternating gabbro, melagabbro, and massive oxide layers. The gabbro of the Lower zone consists of ~40% cumulus clinopyroxene, ~45% plagioclase, ~10 to 15% Fe-Ti oxides, and minor olivine (Song et al., 2013). The Fe-Ti oxides increase gradually up to 85% to form the massive ore layers (Fig. 5e). The massive Fe-Ti oxide ore layers, up to 60 m thick, are mostly restricted to the lower part of this zone. In a few places the massive oxide layers extend from the Lower zone into the Marginal zone. The 300-m-thick Middle zone a is composed of melagabbros with silicate modal composition similar to those in the Lower zone. However, the melagabbros in the Middle zone a have smaller grain sizes and less Fe-Ti oxides than the Lower zone melagabbros. The ore layers in the base of the Middle zone a are 10 m thick. Similar to that in the Hongge intrusion, the clinopyroxene in the Lower zone and Middle zone a of the Panzhihua intrusion also contains ilmenite exsolution lamellae along the [100] planes (Fig. 5f). The 600-m-thick Middle zone b is marked by appearance of cumulus apatite (up to ~5%) and mainly composed of leucogabbros. Olivine also becomes more abundant (10–15%) in this zone (Pang et al., 2008a). The 500- to 1,500-m-thick Upper zone is composed of gabbros and gabbrodiorites. Apatite is absent in the Upper zone. The oxide assemblage in the Marginal zone, Lower zone, and Middle zone a is dominated by titanomagnetite, and ilmenite is rare in these zones (Fig. 5e). In contrast, the Middle zone b and the Upper zone consist of both titanomagnetite and ilmenite in subequal amounts but no ore-grade layer is present in these zones (Pang et al., 2008a).

Similar to the Hongge intrusion, magmatic sulfides are present in the Panzhihua intrusion. The sulfide (dominated by pyrrhotite) abundance in the gabbroic rocks and Fe-Ti oxide layers of the Panzhihua intrusion is up to 5 vol %, but most are less than 2 vol % (Howarth and Prevec, 2013a). All the rocks in the Panzhihua intrusion are depleted in PGE, indicating previous sulfide segregation at depth (Howarth and Prevec, 2013a).

Sampling and Analytical Methods

The intrusive rock samples used in this study were collected from the oxide ore-bearing lithologic units (zones) intercepted by drilling or exposed on the surface at Hongge and Panzhihua. The localities of these samples are shown in the composite lithologic columns in Figures. 3 and 4. The whole-rock, petrography, and electron microprobe data of the Hongge samples have been given in Zhong et al. (2002) and Bai et al. (2012b). The high Ti basalts and the intermediateTi basalts were collected from outcrops in the Longzhoushan (Qi et al., 2008) and Ertan areas (Xu et al., 2001; Fig. 2), respectively. Polished thin sections from the samples were used for in situ mineral chemical analyses. The major plus minor element abundances of Fe-Ti oxides from the intrusive rocks and clinopyroxenes of basalts were determined by wavelength-dispersive X-ray analysis using a JXA-8100 electron microprobe at the State Key Laboratory of Lithospheric Evolution, Institute of Geology and Geophysics, Chinese Academy of Sciences, Beijing, and at the State Key Laboratory of Mineral Deposit Research, Nanjing University. The analytical conditions were 15-kV acceleration voltage, 20-nA beam current, and a beam size of 1-μm diam. Both natural and synthetic oxide and silicate mineral standards were used for calibration. Correction for the interference (peak overlap) of Ti on V was made based on the concentration of Ti in the analyzed minerals.

Major and trace element abundances in the cores of clinopyroxene of the intrusive rocks were determined by spot analysis using an LA-ICP-MS at the State Key Laboratory of Ore Deposit Geochemistry, Institute of Geochemistry, Chinese Academy of Sciences, Guiyang. The ^{23}Na, ^{25}Mg, ^{27}Al, ^{29}Si, ^{42}Ca, ^{45}Sc, ^{49}Ti, ^{51}V, ^{53}Cr, ^{55}Mn, ^{57}Fe, ^{59}Co, ^{60}Ni, ^{65}Cu, ^{66}Zn, ^{71}Ga, ^{88}Sr, ^{89}Y, ^{90}Zr, ^{93}Nb, ^{139}La, ^{140}Ce, ^{141}Pr, ^{143}Nd, ^{147}Sm, ^{151}Eu, ^{155}Gd, ^{159}Tb, ^{163}Dy, ^{165}Ho, ^{166}Er, ^{169}Tm, ^{173}Yb, ^{175}Lu, ^{179}Hf, ^{181}Ta values were determined in clinopyroxene. The instrument conditions, analytical procedures, and data reduction are similar to those given in Liu et al. (2008). Laser sampling was performed using a GeoLasPro laser-ablation system. An Agilent 7700x ICP-MS instrument was used to acquire ion-signal intensities. Helium was applied as a carrier gas. Argon was used as the make-up gas and mixed with the carrier gas via a T connector before entering the ICP. Nitrogen was added into the central gas flow (Ar + He) of the Ar plasma to minimize the detection limit and to improve precision (Hu et al., 2008). The 193-nm ArF excimer laser, homogenized by a set of beam delivery systems, was focused on the target with the energy of 10 J/cm^2. A large beam size of 60 μm was used to ablate both the clinopyroxene and its ilmenite exsolution to avoid the effect of subsolidus exsolution on the clinopyroxene. Each analysis incorporated a background acquisition of approximately 20 to 30 s (gas blank) followed by 40-s data acquisition from the sample. The Agilent Chemstation was utilized for the acquisition of signals. Element abundances were calibrated using multiple reference materials (NIST610, BCR-2G, BIR-1G, and BHVO-2G, GSE-1G) without applying internal standardization (Liu et al., 2008). The reference materials of KL2-G and ML3B-G were analyzed in this study as unknown samples for monitoring the quality of the data. The preferred values of element concentrations for the USGS reference glasses are from the GeoReM database (http://georem.mpch-mainz.gwdg.de/). Off-line selection and integration of background and analytical signals, and time-drift correction and quantitative calibration were performed using the ICPMSDataCal software from Liu et al. (2008, 2010). As illustrated in Figure 6a and b, the

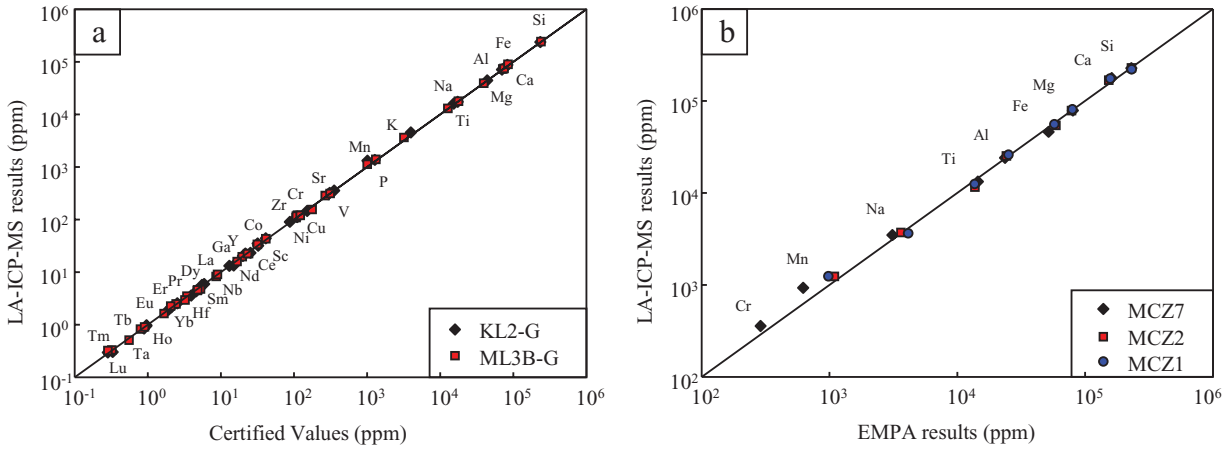

FIG. 6. Comparison of analytical results for international reference materials (a) and clinopyroxene (b).

precisions of the LA-ICP-MS procedure are better than 10% for most elements.

Analytical Results

Oxide inclusions

The compositions of small ilmenite and titanomagnetite crystals enclosed in olivine and clinopyroxene in the samples of the oxide cumulate layers and immediately below oxide cumulate layers in the lower olivine clinopyroxenite zone and the lower subzone of the middle clinopyroxenite zone of the Hongge intrusion are listed in Table 1. The thin (<20 m), subeconomic oxide layers in the lower olivine clinopyroxenite zone are not shown in the composite lithologic column for the Hongge intrusion in Figure 3. The oxide ore layers above sample MCZ14 are shown in Figure 3. The variations of MgO and TiO_2 contents in different types of ilmenite in the Hongge intrusion are shown in Figure 7. The compositions of the ilmenite inclusions are generally similar to those reported by Pang et al. (2008a) but show more scatter than the previous dataset (Fig. 7). The MgO contents of ilmenite inclusions are lower than those of cumulus ilmenite from the overlying oxide cumulate layers (Fig. 7) due to the subsolidus Mg-Fe exchange reaction between ilmenite inclusions and host olivine crystals (Pang et al., 2009). The contents of V_2O_3 and Cr_2O_3 in ilmenite from the Hongge intrusion are below detection limits. The contents of Cr_2O_3 in titanomagnetite inclusions are up to 2.4 wt %, which are similar to the distinct titanomagnetite crystals from the same samples. The contents of Cr_2O_3 in titanomagnetite inclusions are the range of massive ores (0–4.62 wt %) but significantly lower than those of cumulus titanomagnetites in the base of each subzone (up to 13.8 wt %, Bai et al., 2012b). The contents of V_2O_3 in the Hongge titanomagnetite inclusions vary from 0.36 to 1.03 wt %, slightly higher than the V_2O_3 contents in the titanomagnetite of massive ores (0.24–0.75 wt %; Bai et al., 2012b).

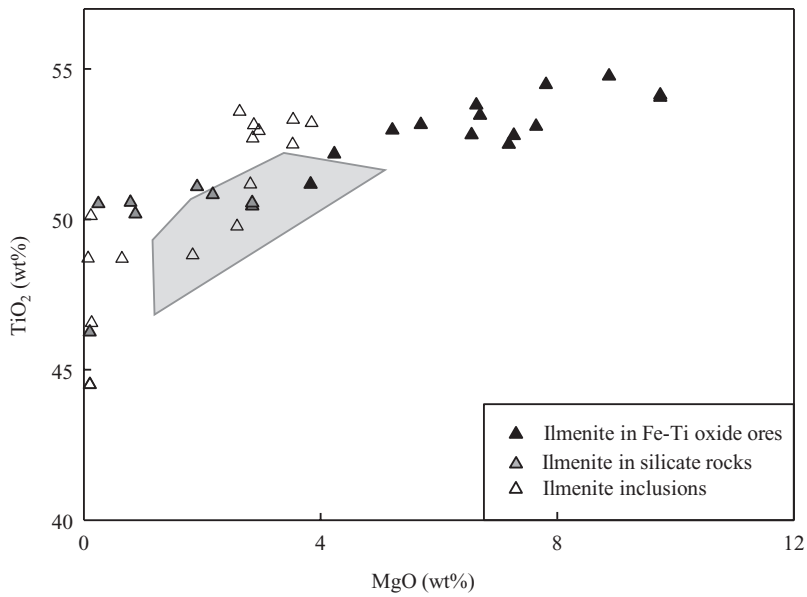

FIG. 7. Plots of MgO vs. TiO_2 contents in ilmenite inclusions from the Hongge intrusion. The compositions of ilmenite in Fe-Ti-V oxide ores and silicate rocks are from Bai et al. (2012b); gray field represents the compositional range of ilmenite inclusions reported by Pang et al. (2008a).

TABLE 1. Compositions of Ilmenite and Magnetite Inclusions in Olivine and Clinopyroxene from the Hongge Intrusion

Sample	Hongge-LOZ5									Hongge-MCZ14					
Rock type	Olivine clinopyroxenite									Clinopyroxenite					
Oxide mineral	Ilmenite							Magnetite		Ilmenite					
Grain	1	2	3	4	5	6	7	1	2	1	2	3	4	5	6
Host	Ol									Cpx					
Host Fo/Mg#	75[1]									75[1]					
MgO	1.84	2.86	2.96	2.87	2.63	2.59	3.53	0.53	0.45	0.10	0.12	0.64	0.13	0.13	0.07
Al_2O_3	0.02	0.00	0.00	0.02	0.00	0.02	0.03	0.73	0.87	0.00	0.01	0.04	0.00	0.11	0.02
NiO	0.00	0.00	0.00	0.03	0.00	0.00	0.00	0.03	0.13	0.00	0.01	0.02	0.00	0.02	0.02
TiO_2	48.81	52.70	52.94	53.14	53.59	49.77	52.50	3.98	2.46	44.51	50.12	48.70	46.85	46.56	48.70
FeO	42.06	42.48	42.59	42.60	43.10	41.26	41.52	33.64	32.63	43.60	46.07	45.04	43.87	45.25	45.83
Fe_2O_3	4.75	1.91	1.91	1.51	1.14	3.87	2.60	56.62	59.97	9.15	2.88	4.9	5.99	7.5	4.28
V_2O_3	0.00	0.00	0.00	0.00	0.00	0.00	0.00	1.00	1.03	0.00	0.00	0.00	0.00	0.00	0.00
MnO	0.70	0.67	0.60	0.71	0.69	0.66	0.58	0.15	0.08	0.38	0.74	0.39	0.72	0.43	0.55
Cr_2O_3	0.03	0.00	0.00	0.00	0.00	0.06	0.00	2.38	2.36	0.00	0.00	0.00	0.00	0.00	0.00
Total	98.22	100.61	101.00	100.88	101.15	98.23	100.76	99.05	99.99	97.79	99.94	99.72	97.56	99.98	99.47
Mg	0.069	0.097	0.108	0.105	0.096	0.104	0.128	0.029	0.024	0.004	0.005	0.024	0.005	0.005	0.003
Al	0.001	0.001	0.000	0.000	0.000	0.000	0.001	0.032	0.037	0.000	0.000	0.001	0.000	0.003	0.001
Ni	0.000	0.000	0.000	0.001	0.000	0.000	0.000	0.001	0.004	0.000	0.000	0.000	0.000	0.000	0.000
Ti	0.929	0.942	0.972	0.978	0.986	0.972	0.962	0.110	0.067	0.860	0.950	0.921	0.909	0.880	0.927
Fe^{2+}	0.890	0.868	0.870	0.872	0.882	0.872	0.846	1.031	0.990	0.937	0.971	0.947	0.947	0.951	0.970
Fe^{3+}	0.096	0.078	0.037	0.030	0.022	0.038	0.051	1.663	1.744	0.189	0.058	0.099	0.124	0.151	0.087
V	0.000	0.000	0.000	0.000	0.000	0.000	0.000	0.062	0.063	0.002	0.000	0.000	0.000	0.000	0.000
Mn	0.015	0.014	0.012	0.015	0.014	0.014	0.012	0.004	0.002	0.008	0.016	0.008	0.016	0.009	0.012
Cr	0.000	0.000	0.000	0.000	0.000	0.000	0.000	0.069	0.068	0.000	0.000	0.000	0.000	0.000	0.000
Total	2.000	2.000	2.000	2.000	2.000	2.000	2.000	3.000	3.000	2.000	2.000	2.000	2.000	2.000	2.000

Sample	Hongge-MCZ14			Hongge-MCZ2								
Rock type	clinopyroxenite			ore								
Oxide mineral	Magnetite			Ilmenite				Magnetite				
Grain	1	2	3	1	2	3	4	1	2	3	4	5
Host	Cpx			Cpx								
Host Fo/Mg#	75[1]			77								
MgO	0.06	0.19	0.22	2.82	3.85	4.64	3.54	1.59	0.75	0.12	0.28	1.87
Al_2O_3	0.31	0.33	0.33	0.01	0.01	0.04	0.02	1.50	2.35	0.37	0.83	2.06
NiO	0.07	0.06	0.06	0.00	0.03	0.00	0.00	0.06	0.00	0.00	0.00	0.02
TiO_2	0.08	0.02	0.09	51.17	53.21	53.43	53.32	10.62	11.50	1.96	3.55	11.69
FeO	30.96	30.74	30.73	40.97	40.54	40.42	41.21	38.21	40.12	32.70	34.21	38.64
Fe_2O_3	67.46	67.60	67.39	2.39	1.39	1.72	0.77	46.52	42.62	63.97	60.94	43.55
V_2O_3	0.75	0.93	0.85	0.00	0.00	0.00	0.00	0.56	0.59	0.77	0.67	0.46
MnO	0.00	0.01	0.00	1.10	1.03	0.37	0.94	0.26	0.34	0.06	0.02	0.30
Cr_2O_3	0.12	0.06	0.11	0.00	0.00	0.00	0.00	0.01	0.01	0.08	0.00	0.00
Total	99.79	99.94	99.77	98.45	100.07	100.62	99.79	99.32	98.27	100.03	100.50	98.57
Mg	0.003	0.010	0.012	0.105	0.141	0.168	0.130	0.086	0.041	0.007	0.015	0.102
Al	0.013	0.014	0.014	0.000	0.000	0.001	0.001	0.064	0.102	0.016	0.036	0.089
Ni	0.002	0.002	0.002	0.000	0.001	0.000	0.000	0.002	0.000	0.000	0.000	0.001
Ti	0.002	0.001	0.003	0.964	0.980	0.972	0.987	0.290	0.318	0.054	0.097	0.320
Fe^{2+}	0.948	0.937	0.939	0.859	0.830	0.818	0.848	1.161	1.235	0.999	1.038	1.178
Fe^{3+}	1.981	1.976	1.975	0.048	0.027	0.033	0.015	1.355	1.257	1.873	1.773	1.273
V	0.046	0.057	0.052	0.000	0.000	0.000	0.000	0.034	0.037	0.048	0.041	0.028
Mn	0.000	0.000	0.000	0.023	0.021	0.008	0.020	0.008	0.011	0.002	0.001	0.009
Cr	0.003	0.002	0.003	0.000	0.000	0.000	0.000	0.000	0.000	0.002	0.000	0.000
Total	3.000	3.000	3.000	2.000	2.000	2.000	2.000	3.000	3.000	3.000	3.000	3.000

Notes: Ol = olivine, Cpx = clinopyroxene; LOZ = lower olivine clinopyroxenite zone, MCZ = middle clinopyroxenite zone
[1] From Bai et al. (2012b)

Clinopyroxene compositions

The average compositions of clinopyroxene from the oxide ore-bearing units (zones) of the Hongge and Panzhihua intrusions, together with the results for the international standards analyzed at the same times, are listed in Table 2. The complete results are given as electronic supplementary material (ESM-1). The Mg number [$Mg/(Mg + Fe^{total})$, molar], TiO_2, and Al_2O_3 contents of clinopyroxene in the Emeishan flood basalts in the Pan-Xi region are also provided as electronic supplementary material (sample ESM-2). A comparison of Mg

Table 2. Average Major and Trace Element Abundances in Core of Clinopyroxene from the Hongge and Panzhihua Intrusions by Spot Analysis of LA-ICP-MS

Intrusion	Hongge						Panzhihua				
Sample	MCZ15	MCZ13	HG0834	MCZ7	MCZ2	MCZ1	PL0602	PL0802	PL0803	PZ0801	PL0603
Zone		MCZa			MCZb				LZ		
Rock type	Cpx	Ore	Ol-cpx	Ore	Ore	Ore	Ore	Ore	Ore	Ore	Gb
No.	6	6	7	7	16	7	4	5	9	5	7
Major oxides (wt %)											
SiO_2	49.19	51.02	51.54	48.60	48.96	47.15	51.84	50.48	50.75	52.11	50.09
TiO_2	1.81	1.78	1.88	2.21	1.93	2.08	1.48	1.58	1.40	1.45	1.49
Al_2O_3	4.20	3.59	4.40	4.55	4.76	4.91	4.32	3.59	3.31	3.22	4.24
FeO^T	5.98	5.80	6.40	5.93	6.98	7.17	7.22	7.36	7.91	7.58	7.57
MnO	0.14	0.13	0.12	0.12	0.16	0.16	0.20	0.25	0.25	0.25	0.24
MgO	13.15	13.45	12.21	13.08	13.08	13.49	12.65	13.34	13.25	12.60	13.37
CaO	24.84	23.67	22.73	24.85	23.49	24.41	21.63	22.70	22.46	22.18	22.31
Na_2O	0.47	0.43	0.43	0.47	0.50	0.49	0.55	0.60	0.56	0.51	0.60
Mg#	80	81	77	80	77	77	76	77	75	75	76
Trace elements (ppm)											
Sc	67.4	61.6	58.3	68.1	57.3	53.8	89.5	77.8	81.6	85.5	87.0
V	308	293	293	327	327	335	280	274	258	250	269
Cr	587	16.4	1022	358	15.9	5.68	32.6	24.5	4.36	6.6	10.2
Co	39.2	38.0	33.6	37.5	34.5	34.1	42.4	40.4	40.0	38.9	40.3
Ni	91.7	68.1	171	78.3	18.8	17.6	17.7	5.95	5.36	5.69	8.12
Cu	0.86	0.81	4.48	1.18	0.69	0.58	1.81	0.75	0.86	0.64	0.90
Zn	33.4	30.5	32.5	28.9	36.4	36.8	33.1	36.2	39.4	48.1	36.2
Ga	10.1	8.51	9.87	10.5	11.1	12.1	9.82	11.4	9.18	9.18	10.1
Sr	178	156	164	144	157	185	55.8	72.7	56.0	59.7	56.2
Y	13.0	11.7	15.1	12.2	19.0	17.2	15.2	18.3	17.0	19.8	17.7
Zr	40.3	33.2	43.3	33.9	51.1	47.4	26.7	25.9	25.1	31.9	29.9
Nb	0.20	0.16	0.28	0.21	0.26	0.29	0.15	0.15	0.12	0.14	-
La	3.71	3.43	4.69	3.17	5.16	5.10	2.23	2.78	2.41	2.34	2.59
Ce	13.8	12.0	16.4	12.2	18.9	18.5	8.90	9.79	9.14	9.36	10.1
Pr	2.78	2.26	3.06	2.49	3.69	3.43	1.76	1.93	1.79	1.89	1.98
Nd	16.3	14.2	18.6	14.7	21.4	21.5	10.5	12.0	11.0	12.4	12.2
Sm	4.84	4.42	5.52	4.35	6.52	6.43	3.70	4.37	4.09	4.56	4.25
Eu	1.60	1.41	1.77	1.43	2.08	2.18	1.47	1.81	1.67	1.90	1.68
Gd	4.80	4.18	5.52	4.23	6.50	6.19	4.31	5.59	4.76	5.48	5.09
Tb	0.64	0.57	0.71	0.59	0.87	0.83	0.62	0.76	0.71	0.80	0.73
Dy	3.36	2.83	3.70	3.03	4.67	4.53	3.47	4.32	4.00	4.66	4.11
Ho	0.57	0.50	0.64	0.52	0.81	0.78	0.65	0.79	0.72	0.84	0.75
Er	1.35	1.12	1.46	1.27	1.95	1.63	1.48	1.78	1.71	1.99	1.76
Tm	0.16	0.11	0.17	0.13	0.22	0.20	0.17	0.23	0.20	0.21	0.20
Yb	0.83	0.72	1.04	0.78	1.26	1.09	1.11	1.29	1.33	1.40	1.28
Lu	0.12	0.10	0.12	0.10	0.16	0.14	0.16	0.18	0.18	0.18	0.17
Hf	2.10	1.80	2.24	1.98	2.66	2.52	1.30	1.43	1.36	1.58	1.46
Ta	0.039	0.036	0.058	0.043	0.052	0.063	0.036	0.032	0.020	0.023	0.020

number, TiO_2 and Al_2O_3 contents in different types of clinopyroxene is illustrated in Figure 8a and b. The results show that at a given Mg number, clinopyroxene phenocrysts from high Ti picrites (TiO_2 >2 wt % in whole rocks) have higher TiO_2 contents than those from intermediate Ti picrites (TiO_2 = 0.8–2 wt % in whole rocks; Kamenetsky et al., 2012). Similarly, at a given Mg number, clinopyroxene crystals from high Ti basalts (TiO_2 >3.5 wt % in whole rocks; e.g., Longzhoushan high TiO_2 basalt; Qi et al., 2008) contain higher TiO_2 than those from intermediate Ti basalts (TiO_2 = 2–3.5 wt % in whole rocks; e.g., the Ertan intermediate TiO_2 basalts; Xu et al., 2001). Our data also show that clinopyroxene phenocrysts of the basalts have higher Mg numbers than coexisting clinopyroxene crystals in the groundmass. Both types of clinopyroxene from each type of basalts collectively produce a clear, negative TiO_2–Mg number correlation that is consistent with fractional crystallization. The average clinopyroxene Mg number and TiO_2 contents of individual samples from the oxide ore-bearing lithologic units (zones) of the Hongge intrusions are 77 to 81 and 1.7 to 2.2 wt%, respectively. These values are within the ranges of clinopyroxene crystals from coeval high Ti basalts (Fig. 8a). The average clinopyroxene Mg nunber and TiO_2 contents of individual samples from the oxide ore-bearing lithologic units (zones) of the Panzhizhua intrusions are 74 to 77 and 1.2 to 1.6 wt %, respectively. These values are within the ranges of clinopyroxene crystals from coeval intermediate Ti basalts (Fig. 8a). The Al content of clinopyroxene is an important control on partitioning of other elements (due to charge balance) and also an indicator of silica activity (Campbell and Borley, 1974). Generally, there is no clear correlation between Mg number and Al_2O_3 contents in clinopyroxene and no regular contrast of Al_2O_3 content between high

Table 2. *(Cont.)*

Intrusion	Panzhihua			Reference material							
Sample	PL0804	PZ0601	PZ0605	BHVO-2G			BIR-1G			BCR-2G	
Zone		MCZa									
Rock type	Ore	Ore	Ore	Measured	Stdev	Certified	Measured	Stdev	Certified	Measured	Stdev
No.	3	6	6		4			4		4	
Major oxides (wt %)											
SiO	50.60	49.35	50.00	51.46	0.310	49.31	49.22	0.408	47.51	56.5	0.265
TiO_2	1.26	1.42	1.53	2.52	0.018	2.72	0.86	0.005	0.9	2.12	0.005
Al_2O_3	3.11	3.89	3.72	13.61	0.359	13.60	15.43	0.419	15.5	13.7	0.379
$FeO_{(total)}$	8.28	8.57	7.81	9.91	0.093	11.30	9.07	0.074	10.4	11.3	0.000
MnO	0.26	0.26	0.25	0.18	0.000	0.17	0.18	0.000	0.19	0.21	0.005
MgO	13.25	13.65	13.67	7.13	0.037	7.13	9.53	0.041	9.4	3.52	0.054
CaO	22.58	22.16	22.35	11.79	0.141	11.40	13.47	0.058	13.3	7.32	0.045
Na_2O	0.54	0.60	0.57	2.44	0.026	2.40	1.99	0.013	1.85	3.38	0.045
Mg#	74	74	76								
Trace elements (ppm)											
Sc	81.5	84.4	83.9	36.0	2.07	33.0	47.3	2.05	43	38.9	2.38
V	249	248	278	325	5.74	308	330	4.11	326	430	10.17
Cr	8.57	7.12	9.30	316	1.71	293	434	8.16	392	15.7	1.46
Co	40.3	37.9	38.6	47.0	0.801	44	55.7	1.05	52	38.2	1.10
Ni	6.52	4.77	9.52	130	1.50	116	187	2.65	178	11.6	0.79
Cu	0.90	2.27	0.57	135	1.26	127	133	2.87	119	16.8	1.66
Zn	39.8	39.8	43.6	121	4.79	102	89	0.435	78	162	5.00
Ga	9.11	10.4	11.1	24.6	0.465	22.0	17	0.173	15	23.7	0.275
Sr	58.7	58.3	55.6	389	10.5	396	107	1.29	109	346	6.35
Y	17.2	18.8	19.0	23.3	0.548	26.0	13.4	0.332	14.3	32.1	0.311
Zr	25.0	31.3	34.9	157	3.42	170	13	0.392	14	176	3.916
Nb	0.130	0.14	0.14	16.0	0.591	18.3	0.35	0.519	0.52	11.2	0.236
La	2.23	2.73	3.01	15.6	0.427	15.2	0.65	0.037	0.61	26.2	0.733
Ce	8.76	10.1	10.7	36.7	0.789	37.6	2.02	0.081	1.89	52.1	0.150
Pr	1.74	1.98	2.12	5.11	0.141	5.35	0.28	0.068	0.37	6.47	0.156
Nd	11.1	12.9	13.2	24.9	0.804	24.5	2.01	0.603	2.37	27.3	0.834
Sm	3.96	4.63	4.59	5.9	0.207	6.1	0.9	0.049	1.09	6.15	0.401
Eu	1.76	1.86	1.78	2.09	0.099	2.07	0.64	0.029	0.517	2.4	0.156
Gd	4.84	5.46	5.49	6.31	0.271	6.16	1.48	0.150	1.85	7.04	0.700
Tb	0.69	0.75	0.78	0.93	0.025	0.92	0.31	0.024	0.35	1	0.037
Dy	4.08	4.38	4.37	4.85	0.225	5.28	2.34	0.090	2.55	6.48	0.382
Ho	0.73	0.81	0.84	0.89	0.079	0.98	0.56	0.030	0.56	1.24	0.074
Er	1.72	1.86	1.88	2.27	0.145	2.56	1.42	0.176	1.7	3.61	0.176
Tm	0.20	0.22	0.24	0.31	0.030	0.34	0.25	0.013	0.24	0.5	0.017
Yb	1.26	1.35	1.33	2.19	0.091	2.01	1.44	0.085	1.64	3.43	0.344
Lu	0.15	0.17	0.19	0.24	0.028	0.28	0.24	0.026	0.25	0.43	0.052
Hf	1.30	1.51	1.82	4.40	0.182	4.32	0.54	0.132	0.57	4.83	0.318
Ta	0.015	0.028	0.025	1.11	0.056	1.15	0.022	0.023	0.036	0.73	0.017

and intermediate Ti basalts (Fig. 8b). At a given Mg number, clinopyroxenes from the Hongge intrusion have slight higher Al_2O_3 contents than those from the Panzhihua intrusion but overlap each other. Similarly, at a given Mg number, the Al_2O_3 content of clinopyroxene crystals from high Ti basalts (TiO_2 >3.5 wt % in whole rocks; e.g., Longzhoushan high TiO_2 basalts; Qi et al., 2008) overlap those from intermediate Ti basalts (TiO_2 = 2–3.5 wt % in whole rocks; e.g., the Ertan intermediate TiO_2 basalts; Xu et al., 2001). In contrast, at a given Mg number, clinopyroxene phenocrysts from high Ti picrites (TiO_2 >2 wt % in whole rocks) have much lower Al_2O_3 contents than those from intermediate Ti picrites (TiO_2 = 0.8–2 wt % in whole rocks; Kamenetsky et al., 2012; Fig. 8b). As shown in Figure 9, clinopyroxene crystals from the Hongge and Panzhuhua oxide ore-bearing lithologic units (zones) have different Cr, V, Nb, Zr, Ce, and Nd concentrations. The highly variable Cr contents in clinopyroxene and magnetite of the Hongge intrusion are probably due to fractional crystallization of Fe-Ti oxides. Chrome partitions strongly into magnetite due to its high partition coefficient between magnetite and silicate melt ($D_{Cr}^{Mt/liq}$ = 153, Rollinson, 1993). As a result, Cr would decrease quickly in the residual magma during fractional crystallization of magnetite (McCarthy and Cawthorn, 1983).

At a given Mg number, the concentrations of the incompatible elements in clinopyroxene tend to be higher for the Hongge intrusion than those for the Panzhihua intrusion (Fig. 9). The clinopyroxene crystals from the Hongge oxide ore-bearing units show more fractionated REE patterns than those from Panzhihua (Fig. 10a). The trace element patterns of clinopyroxenes from these two intrusions are also different (Fig. 10b). Specifically, the abundances of high field strength

TABLE 2. *(Cont.)*

Intrusion	Reference material										D.L.
Sample	BCR-2G	GSE-1G		KL2-G			ML3B-G				
Zone											
Rock type	Certified	Measured	Stdev	Certified	Measured	Stdev	Certified	Measured	Stdev	Certified	
No.		4			8				8		
Major oxides (wt %)											
SiO	54.41	55.4	0.294	53.7	50.85	0.381	50.30	52.02	0.509	51.40	0.0878
TiO_2	2.35	0.07	0.001	0.08	2.67	0.052	2.56	2.17	0.056	2.13	0.0010
Al_2O_3	13.4	13.6	0.386	13	13.42	0.376	13.30	13.77	0.453	13.60	0.0005
$FeO_{(total)}$	12.4	11.2	0.082	12.7	11.20	0.524	10.70	11.49	0.581	10.90	0.0048
MnO	0.2	0.08	0.001	0.08	0.18	0.005	0.17	0.18	0.000	0.17	0.0002
MgO	3.56	3.4	0.077	3.48	7.35	0.172	7.34	6.55	0.135	6.59	0.0055
CaO	7.06	7.62	0.117	7.42	10.89	0.177	10.90	10.51	0.139	10.50	0.0689
Na_2O	3.23	4.26	0.017	3.91	2.33	0.030	2.35	2.40	0.019	2.40	0.0048
Mg#											
Trace elements (ppm)											
Sc	33	523	11.15	530	34.9	2.17	31.8	33.9	1.97	31.6	0.10
V	425	425	7.14	440	320	8.32	309	287	6.27	268	0.023
Cr	17	408	7.14	400	303	8.40	294	156	5.63	177	0.43
Co	38	386	2.08	380	43.9	0.66	41.2	43.2	0.991	41.2	0.026
Ni	13	461	3.86	440	114	5.83	112	109	3.40	107	0.34
Cu	21	392	9.33	380	90.5	2.97	87.9	121	4.54	112	0.46
Zn	125	491	12.48	460	111	4.50	110	117	4.78	108	0.43
Ga	23	582	4.08	490	20.3	0.790	20.0	19.7	0.528	19.6	0.042
Sr	342	457	10.47	447	356	7.70	356	313	8.77	312	0.020
Y	35	418	5.44	410	23.3	0.614	25.4	22.5	0.583	23.9	0.014
Zr	184	408	6.03	410	146	3.65	152	121	2.95	122	0.028
Nb	12.5	398	9.22	420	13.4	0.583	15.0	8.29	0.241	8.61	0.014
La	24.7	416	9.46	392	13.2	0.480	13.1	9.04	0.444	8.99	0.011
Ce	53.3	417	2.38	414	31.8	0.729	32.4	22.5	0.608	23.1	0.010
Pr	6.7	452	9.00	460	4.32	0.208	4.60	3.50	0.155	3.43	0.012
Nd	28.9	461	2.94	453	22.6	1.07	21.6	15.9	0.676	16.7	0.063
Sm	6.59	494	5.50	488	5.72	0.469	5.54	4.50	0.342	4.75	0.130
Eu	1.97	435	6.48	410	1.93	0.12	1.92	1.63	0.072	1.67	0.027
Gd	6.71	510	8.54	490	5.94	0.283	5.92	4.76	0.302	5.26	0.056
Tb	1.02	507	8.35	480	0.85	0.072	0.89	0.83	0.035	0.80	0.015
Dy	6.44	525	11.20	524	5.07	0.194	5.22	4.62	0.435	4.84	0.067
Ho	1.27	520	10.72	501	0.98	0.024	0.96	0.91	0.060	0.91	0.014
Er	3.7	476	41.62	595	2.56	0.260	2.54	2.48	0.183	2.44	0.021
Tm	0.51	507	7.79	500	0.30	0.030	0.33	0.33	0.023	0.32	0.015
Yb	3.39	526	6.13	520	2.15	0.244	2.10	2.27	0.169	2.06	0.042
Lu	0.5	529	13.28	518	0.30	0.024	0.29	0.32	0.052	0.29	0.011
Hf	4.84	414	13.44	395	3.59	0.358	3.93	2.96	0.177	3.22	0.054
Ta	0.78	426	8.70	390	0.95	0.057	0.96	0.51	0.043	0.56	0.007

Abbreviations: Ore = Fe-Ti oxide ore, Cpx = clinopyroxenite, Ol-cpx = olivine clinopyroxenite, Gb = gabbro, Stdev = standard deviation, DL = detection limit; Mg# = [100*MgO/(MgO + $_{FeO(total)}$, molar)]; MCZa = middle clinopyroxenite zone a, MCZb = middle clinopyroxenite zone b

trace element are higher in clinopyroxene from the Hongge intrusion than those from Panzhihua.

Modeling and Discussion

Origin of ilmenite inclusions in olivine and clinopyroxene

Pang et al. (2008a) concluded that ilmenite-magnetite inclusions in the Hongge intrusion and magnetite inclusions in the Panzhihua intrusion are neither xenocrysts nor immiscible melt but primocrysts entrapped by olivine and clinopyroxene during crystallization. Experiments have shown that ilmenite can crystallize directly from high Ti basaltic magma (Snyder et al., 1993; Toplis and Carroll, 1995; Botcharnikov et al., 2008). In mafic intrusions, ilmenite may also form by subsolidus exsolution from Fe-Ti spinel on cooling. Ilmenite inclusions within olivine and clinopyroxene crystals and ilmenite cumulates in mafic intrusions are commonly regarded as textural evidence for the former, whereas exsolution lamellae or fine-grained intergrowth with magnetite are used as textural evidence for the latter (e.g., Cawthorn et al., 1985, 1989; Cawthorn and Biggar, 1993; Pang et al., 2008a, b). Ilmenite phenocrysts have been found in picritic basalts elsewhere in the world such as the Karoo flood basalt province (Cawthorn et al., 1989) and the Siberian and Deccan Traps (Murari et al., 1993). In the Hongge intrusion, the occurrence of ilmenite inclusions in olivine (Fig. 5a, b) is consistent with

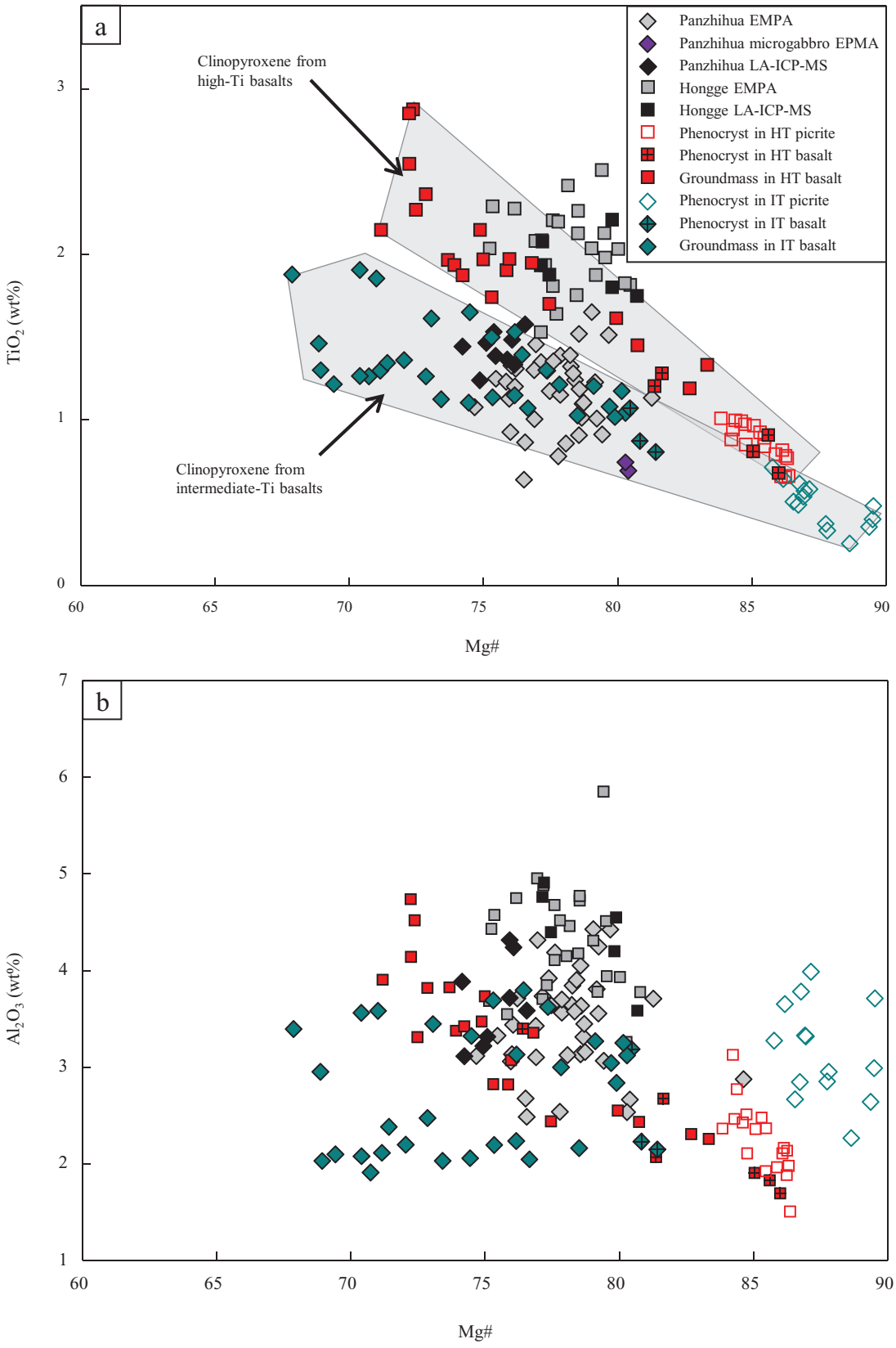

FIG. 8. Comparison of clinopyroxene TiO_2-Mg number relationships for the Hongge and Panzhihua intrusions, and coeval volcanic rocks. The results determined by EMPA for the Hongge and Panzhihua intrusions are from Bai et al. (2012b) and Pang et al. (2009). The compositions of clinopyroxene in the Emeishan picrites are from Kamenetsky et al. (2012). The compositions of clinopyroxene in the selected basaltic samples are given in supplementary Table 2.

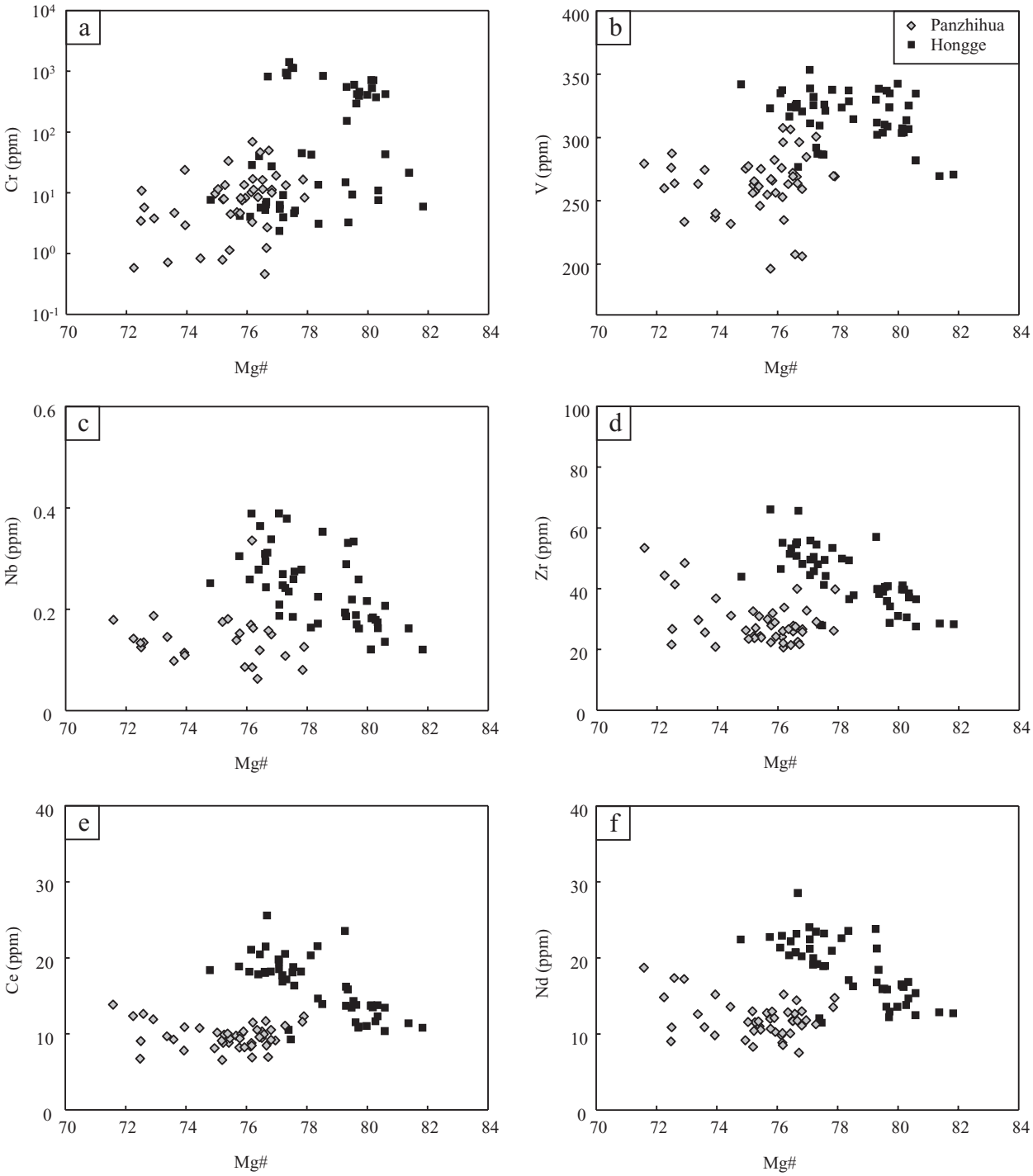

FIG. 9. Plots of Mg number vs. Cr (a), V (b), Nb (c), Zr (d), Ce (e), and Sr (f) in clinopyroxene from the Hongge and Panzhihua intrusions.

the interpretation that this type of ilmenite formed by cotectic crystallization with silicates.

Whole-rock compositional variations of oxide-rich samples from the Hongge and Panzhihua intrusions are consistent with a cumulus origin for the oxide-rich layers. The variations of $FeO_{(total)}$, TiO_2, and V contents in the oxide-rich samples from these intrusions are clearly controlled by ilmenite + titanomagnetite or titanomagnetite (Fig. 11a, b). Data from this study and from Pang et al. (2008a, b) show that the oxide inclusions in olivine and clinopyroxene crystals from the Panzhihua intrusion are dominated by titanomagnetite, whereas both magnetite and ilmenite inclusions are present in olivine and clinopyroxene crystals from the Hongge intrusion.

Cumulus ilmenite in the Hongge intrusion contains up to 9.7 wt % MgO (Bai et al., 2012b), similar to Mg-rich ilmenite phenocrysts in picritic basalts from the Karoo flood basalt

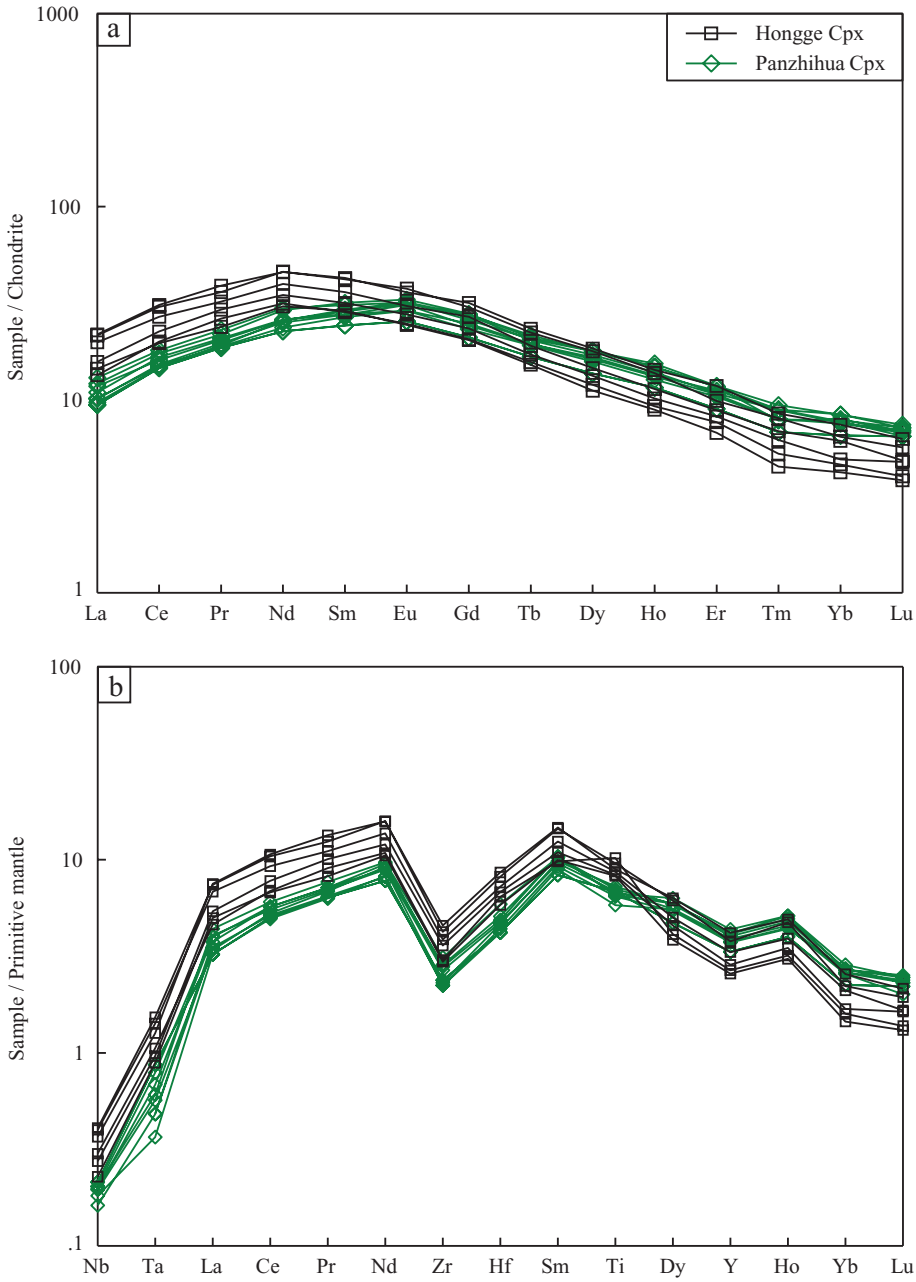

FIG. 10. Chondrite-normalized REE patterns (a) and primitive mantle-normalized alteration-resistant trace element patterns (b) for clinopyroxene from the Hongge and Panzhihua intrusions. The values for chondrite and primitive mantle are from Sun and McDonough (1989).

province (Cawthorn and Biggar, 1993). Based on the results from the Insizwa mafic-ultramafic intrusion in the Karoo igneous province, Cawthorn and Biggar (1993) suggested high Ti parental magma with approximately 5 wt % MgO for Mg-rich ilmenite. The lower MgO contents of the Hongge ilmenite inclusions relative to the cumulus ilmenite from the overlying oxide cumulate layers (Fig. 7) may have resulted from subsolidus Mg-Fe exchange reaction between ilmenite inclusion and the host olivine. This is consistent with the observation that olivine in the massive ores has much higher Fo than that in the associated oxide-poor rocks of the Hongge and Panzhihua deposits (Pang et al., 2009; Bai et al., 2012b). Hence, we regard ilmenite inclusions within olivine crystals with Fo >77 (Bai et al., 2012b) in the Hongge intrusion as evidence for high Ti basaltic parental magma.

Based on the observations from the Bushveld Complex and the Skaergaard layered intrusion, several researchers suggested that Mg-poor ilmenite and titanomagnetite could crystallize together from evolved magma (McBirney, 1989, 1996; Tegner et al., 2006, 2009; Thy et al., 2009). We suggest that the interstitial ilmenite-titanomagnetite-apatite assemblages in the upper zones of the Hongge and Panzhihua intrusions formed from magma that is more fractionated than the parental magma of the underlying oxide layers.

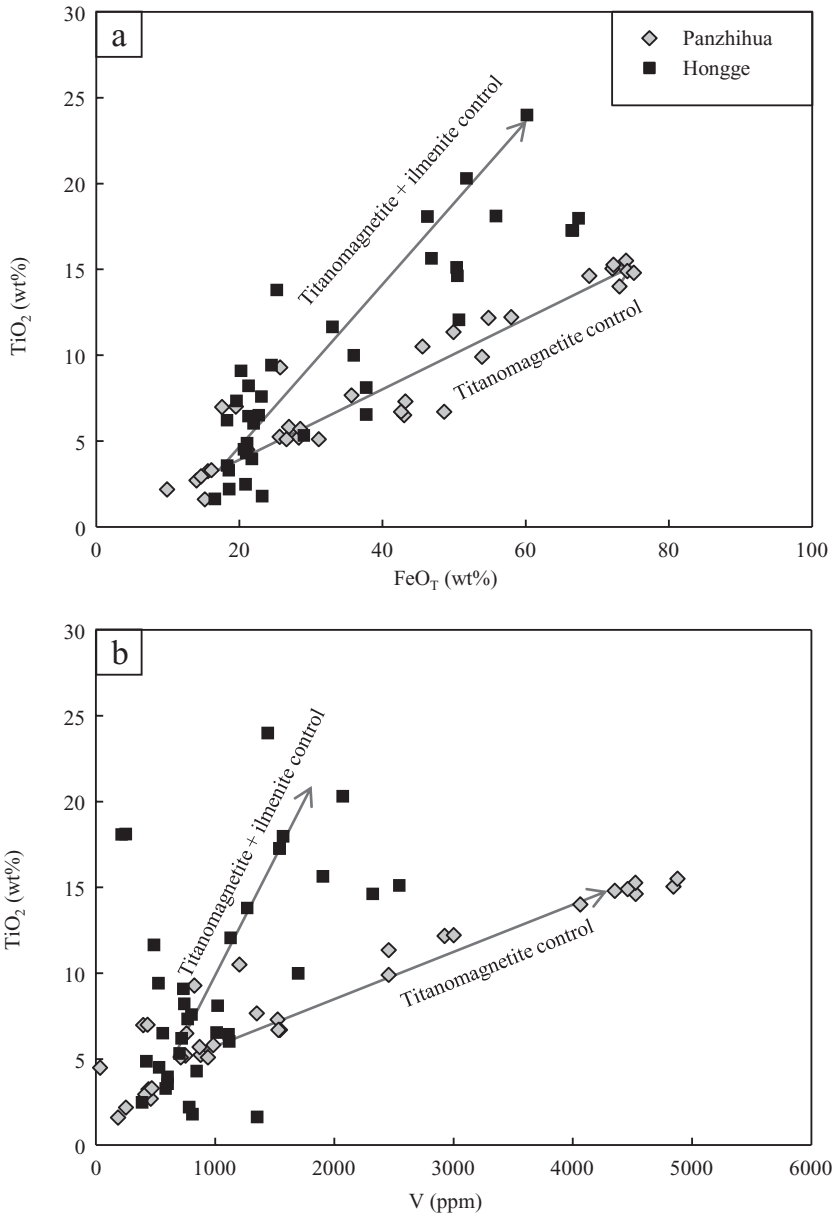

FIG. 11. Plots of $FeO_{(total)}$ vs. TiO_2 (a) and V (b) in whole-rock samples with La contents <10 ppm from the main ore horizons of the Hongge and Panzhihua intrusions. Data for the Hongge intrusion are from Zhong et al. (2002) and Bai et al. (2012b); data for the Panzhihua intrusion are from Zhou et al. (2005) and Pang (2008).

Estimation of liquid TiO_2 contents and MgO/FeO ratios

The major and incompatible trace element concentrations in cumulus phases in intrusive rocks may have been modified by reequilibration with trapped liquids (Barnes, 1986; Godel et al., 2011; Cawthorn, 2013). Using whole-rock Zr contents, Pang et al. (2009) estimated up to 20 wt % trapped liquid for the Panzhihua cumulate rocks and up to 7 mol % Mg number trapped liquid shift for clinopyroxene in the rocks. These values are likely overestimated because Zr is compatible in magmatic Fe-Ti oxides (Nielsen and Beard, 2000). Rare earth elements that are incompatible in both silicate minerals and coexisting oxides are better choices for the estimation. Thus, we have used a rare earth element, La, to estimate the proportions of trapped liquids in the Hongge and Panzhihua samples. The results are shown in Figure 12. The massive ores from the Hongge and Panzhihua deposits contain similarly low La contents (<2 ppm; Zhou et al., 2005; Pang, 2008; Bai et al., 2012; Luan et al., 2014). Using the average content of La in the Emeishan high Ti basalts (45 ppm; Qi et al., 2008) to represent the liquid composition, the amounts of trapped liquid in the massive oxide ore samples from both deposits are estimated to be <5 wt %. Such extremely low proportions of trapped liquid would have negligible effect on incompatible trace element compositional variation in the cumulus clinopyroxene crystals. More importantly, the proportions of trapped liquids in the oxide layers of both intrusions are similar (Fig. 12). It is therefore expected that the trapped liquid shifts of incompatible trace element abundances in the cumulus

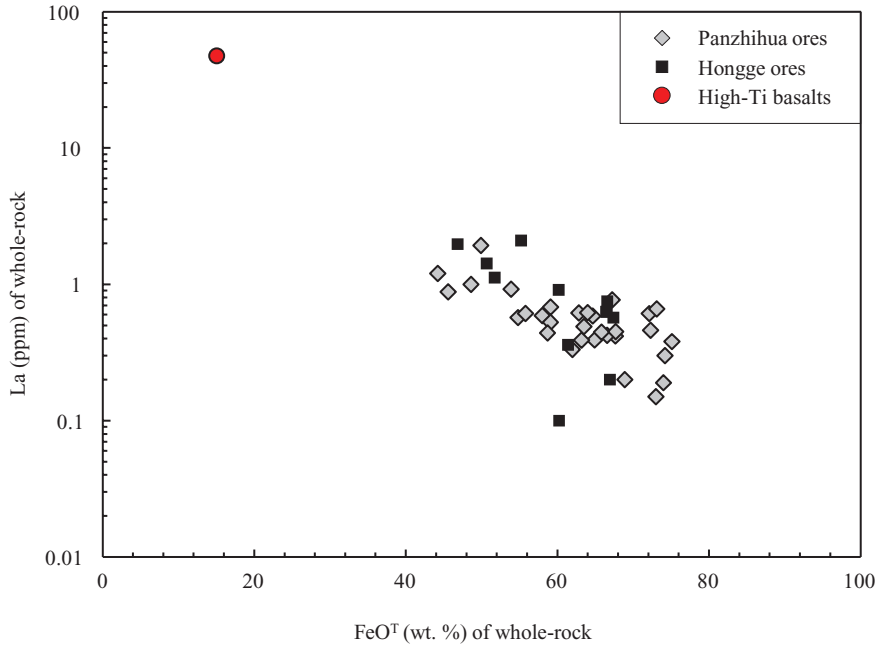

FIG. 12. Plots of La vs. $FeO_{(total)}$ in massive Fe-Ti oxide ores, showing that the ore samples from the Hongge and Panzhihua deposits contain similarly lowtrapped liquids. The data for the massive ores are from Zhong et al. (2002), Zhou et al. (2005), Bai et al. (2012b), Pang (2008), Song et al. (2013), and Luan et al. (2014). The data for the Emeishan high Ti basalts are from Qi et al. (2008, their sample LZS-37).

clinopyroxene crystals from both intrusions are similar and negligible.

The Mg# values of clinopyroxene from massive oxide layers and adjacent clinopyroxenites and gabbros in the Hongge and Panzhihua intrusions are similar (Pang et al., 2009; Bai et al., 2012b), indicating that subsolidus reequilibration between clinopyroxene and oxides is insignificant. Experimental work (Cherniak and Liang, 2012) has shown that Ti diffusion in pyroxene is very slow. This explains why Ti zonation in pyroxene crystals from layered intrusions such as the Bushveld Complex is common (Godel et al., 2011). Although no Ti zonation was investigated in this study since we only analyzed the core of clinopyroxene, the Ti content of the core would not shift by trapped liquid or subsolidus reequilibration due to its slow diffusion. Similar TiO_2–Mg number relationships for the clinopyroxene crystals from both intrusive and extrusive rocks in the Emeishan large igneous province (see Fig. 8) provide additional evidence that the effect of subsolidus reequilibration on the contents of TiO_2 and Mg number in the cumulus clinopyroxene crystals from the Hongge and Panzhihua intrusions are negligible. Hence, the contents of TiO_2 in the parental magmas of these deposits can be estimated from the contents of TiO_2 in the cumulus clinopyroxene crystals associated with the ores. Using the average experimentally determined partition coefficient of 0.45 for TiO_2 between clinopyroxene and basaltic magma from Hauri et al. (1994), the concentrations of TiO_2 in the parental magmas for the oxide ore layers of the Hongge and Panzhihua intrusions are estimated to be 3.9 to 4.9 and 2.8 to 3.5 wt %, respectively. The former are similar to the compositions of the Emeishan large igneous province high Ti basalts at Longzhoushan (up to 4.5 wt % TiO_2; Qi et al., 2008); the latter are similar to the compositions of the Emeishan large igneous province intermediate Ti basalts at Ertan (2.37–3.47 wt % TiO_2; Xu et al., 2001).

Oxygen state is known to have a significant influence on the liquidus of Fe-Ti spinel in mafic magma (Toplis and Carroll, 1995). This has let many researchers (Ganino et al., 2008; Pang et al., 2008a; Bai et al., 2012b) suggest that the relatively early arrival of Fe-Ti oxides in the Panzhihua and Hongge magmatic systems as compared to other layered intrusions in the world was caused by higher oxidation states. Different oxidation states may have contributed to the contrasting oxide assemblages between the Hongge deposit (titanomagnetite and ilmenite) and the Panzhihua deposit (mainly titanomagnetite). However, the occurrence of magmatic sulfides in both deposits indicates that the oxidation states of these two magmatic systems were all below FMQ +1.5. Sulfide is not stable in mafic magma at an oxidation state above FMQ +1.5 (Jugo et al., 2005). The results from oxide chemistry have shown that the Hongge and Panzhihua deposits formed under similar oxidation states between FMQ +1 and FMQ +1.5 (Pang et al., 2008a; Bai et al., 2012b).

Experiments show that the crystallization of ilmenite from ferrobasaltic magma is mainly controlled by TiO_2 content in the magma (Toplis and Carroll, 1995). Under geologically reasonable conditions, ilmenite and titanomagnetite will appear on the liquidus together with clinopyroxene if the content of TiO_2 in basaltic magma is >4 wt %, titanomagnetite will appear on the liquidus together with clinopyroxene if the content of TiO_2 in the magma is lower (Snyder et al., 1993; Toplis and Carroll, 1995; Botcharnikov et al., 2008). We suggest that the contrasting oxide assemblages between the Hongge and Panzhihua deposits are mainly due to different TiO_2 contents in the parental magmas instead of different oxidation states.

Using the average Fe-Mg exchange coefficient between clinopyroxene and melt, or $Kd^{Cpx/melt} = (FeO/MgO)^{Cpx}/(FeO/MgO)^{melt}$), of 0.27 from Bédard (2010) and the compositions of most primitive clinopyroxene crystals (highest Mg numbers) from the Hongge and Panzhihua intrusions, the MgO/FeO ratios in the parental magmas for these two intrusions are estimated to be 0.63 and 0.49, respectively. These are minimum values because the MgO/FeO ratios in the clinopyroxene have been modified by trapped liquid and subsolidus reequilibration with coexisting oxides. As described above, the estimated amounts of trapped liquids in the samples from both deposits are similar and lower than 5 wt %. This means that the trapped liquid shifts for clinopyroxene MgO/FeO from both deposits are similar and small; probably less than 1% relative change in MgO/FeO based on the calculations of Barnes (1986). Since the samples from both deposits contain similar amount oxides, the effect of subsolidus reequilibration with coexisting oxides on the cumulus clinopyroxene crystals from both deposits are also similar. Hence, the different liquid MgO/FeO ratios estimated from cumulus clinopyroxene compositions mainly reflect the difference in the parental magmas of these deposits.

Our calculations based on the average composition of most primitive clinopyroxene from both deposits show that the parental magma for the Hongge deposit has significantly higher MgO/FeO than that for the Panzhihua deposit. As described above, the parental magma for the Hongge deposit also has higher TiO_2 content than that for the Panzhihua deposit. These results together indicate that the parental magmas of these two deposits could not be related to each other by fractional crystallization because such a process would produce a negative MgO/FeO-TiO_2 correlation.

Estimation of liquid trace element compositions

Figure 13 illustrates the primitive mantle-normalized patterns for selected trace elements of the parental magmas estimated for the Hongge and Panzhihua ore-bearing intrusions and selected flood basalts in the Emeishan large igneous province. The abundances of selected trace elements in the magmas are estimated using the average compositions of clinopyroxene from the ore-bearing lithologic units (zones) of the intrusions and the Cpx/liquid partition coefficients determined experimentally by Hart and Dunn (1993), Hauri et al. (1994), Lundstrom et al. (1998), Hill et al. (2000), and Gaetani et al. (2003). The results show that the estimated trace element compositions of the Hongge and Panzhihua magmas are similar to the compositions of high Ti basalts at Longzhoushan and intermediate Ti basalts at Ertan, respectively (Fig. 13). The estimated trace element compositions of the parental magma for the Panzhihua deposit are remarkably similar to a microgabbro from the margin of the intrusion (Zhou et al., 2005). As shown in Figure 13, the normalized trace element pattern of the Hongge magma is clearly more fractionated than that of the Panzhihua magma. The former have higher LREE and HFSE abundances than the latter. These enrichments may be due to fractional crystallization of clinopyroxene. However, as described above, clinopyroxene in the Hongge intrusion is more primitive than that in the Panzhihua intrusion. Thus, the different trace element patterns mainly reflect different

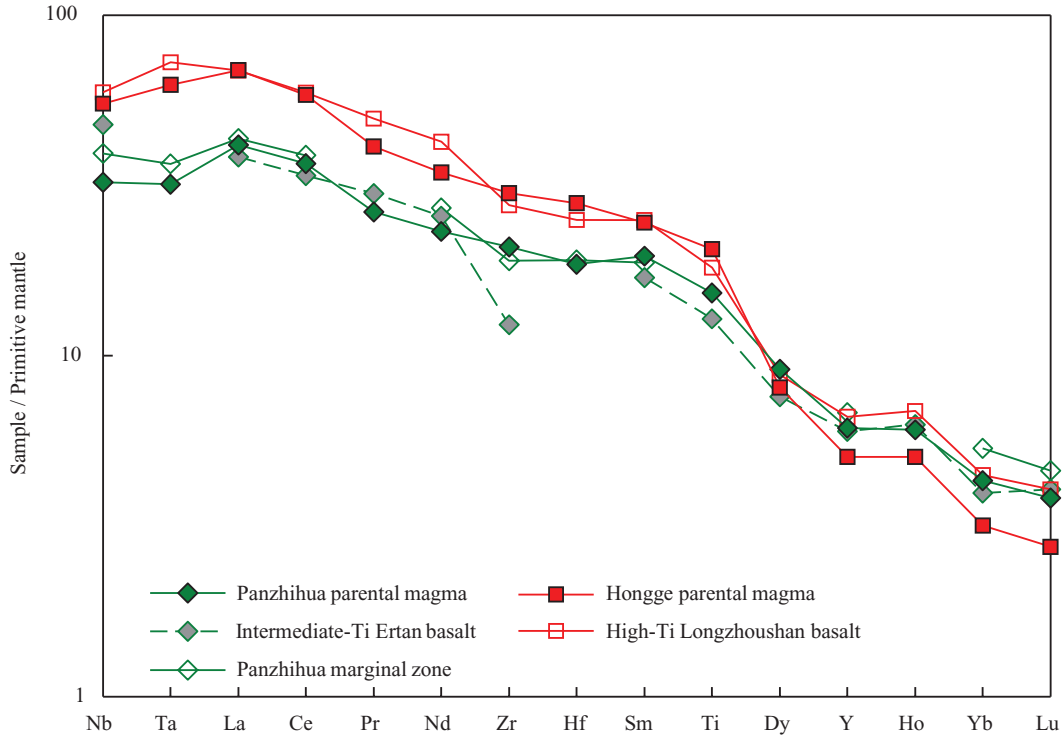

FIG. 13. Comparison of liquid trace element compositions calculated from average compositions of clinopyroxene from the main ore horizons in the Hongge and Panzhihua intrusions with the compositions of selected Emeishan basalts and a samples from the marginal zone of the Panzhihua intrusion. Data sources: intermediate Ti basalt Ertan (Xu et al., 2001, their sample EM-82); Panzhihua marginal zone (Zhou et al., 2005, their sample LJ-03); high Ti basalt from Longzhoushan, (Qi et al., 2008, their sample LZS-37).

parental magma compositions. Different trace element patterns also present among the Emeishan picrites, which are attributed to source variations (Kamenetsky et al., 2012; Li et al., 2012).

Many researchers (Zhou et al., 2005; Pang et al., 2008a; Zhang et al., 2009; Bai et al., 2012b; Song et al., 2013; Luan et al., 2014) suggested that the Hongge and Panzhihua magmas are similar to the Emeishan high Ti basalts. Recently, Howarth and Prevec (2013b) suggested that the parental magma of the Panzhihua intrusion is similar to the lower end of TiO_2 content for typical Emeishan high Ti basalts (2.5 wt % TiO_2). The average compositions of high Ti basalts from Longzhoushan and intermediate Ti basalts from Ertan can be used to represent the compositions of the parental magmas for the Hongge and Panzhihua deposits, respectively, in agreement with the modeling of Howarth and Prevec (2013b).

Origins of contrasting parental magma compositions

Traditionally, Sr-Nd isotope variations between the Hongge and Panzhihua intrusions are attributed to variable degrees of contamination with the upper crust (e.g., Zhong et al., 2003; Zhou et al., 2008; Zhang et al., 2009). In this model, the Hongge magma is thought to have experienced significantly higher degrees of contamination than the Panzhihua magma (Fig. 14a). This model can explain the isotope data but cannot explain different mineral assemblages and mineral chemistry between these two intrusions. As described above, plagioclase is common in the Panzhihua intrusion but is absent to rare in the more primitive Hongge intrusion. Orthopyroxene is also absent in the Hongge intrusion. The mineral assemblages do not support the model of a higher degree of siliceous contamination for the Hongge magma than the Panzhihua magma. It is well known that the addition of SiO_2 to mafic magma favors the crystallization of orthopyroxene and plagioclase at the expense of olivine and clinopyroxene (Irvine, 1970; Sparks, 1986). Additionally, the insignificantly contaminated Emeishan picrites exhibit large variations in ε_{Nd} and incompatible trace elements, implying mantle source heterogeneity (Li et al., 2012).

The forgoing analysis demonstrates that fractional crystallization and variable degrees of contamination with the upper crust cannot fully explain the contrasting compositions of the estimated parental magmas for the Hongge and Panzhihua intrusions. The variations of TiO_2 content and trace elements in the Emeishan picrites and associated basalts have been proposed to be generated by different degrees of partial

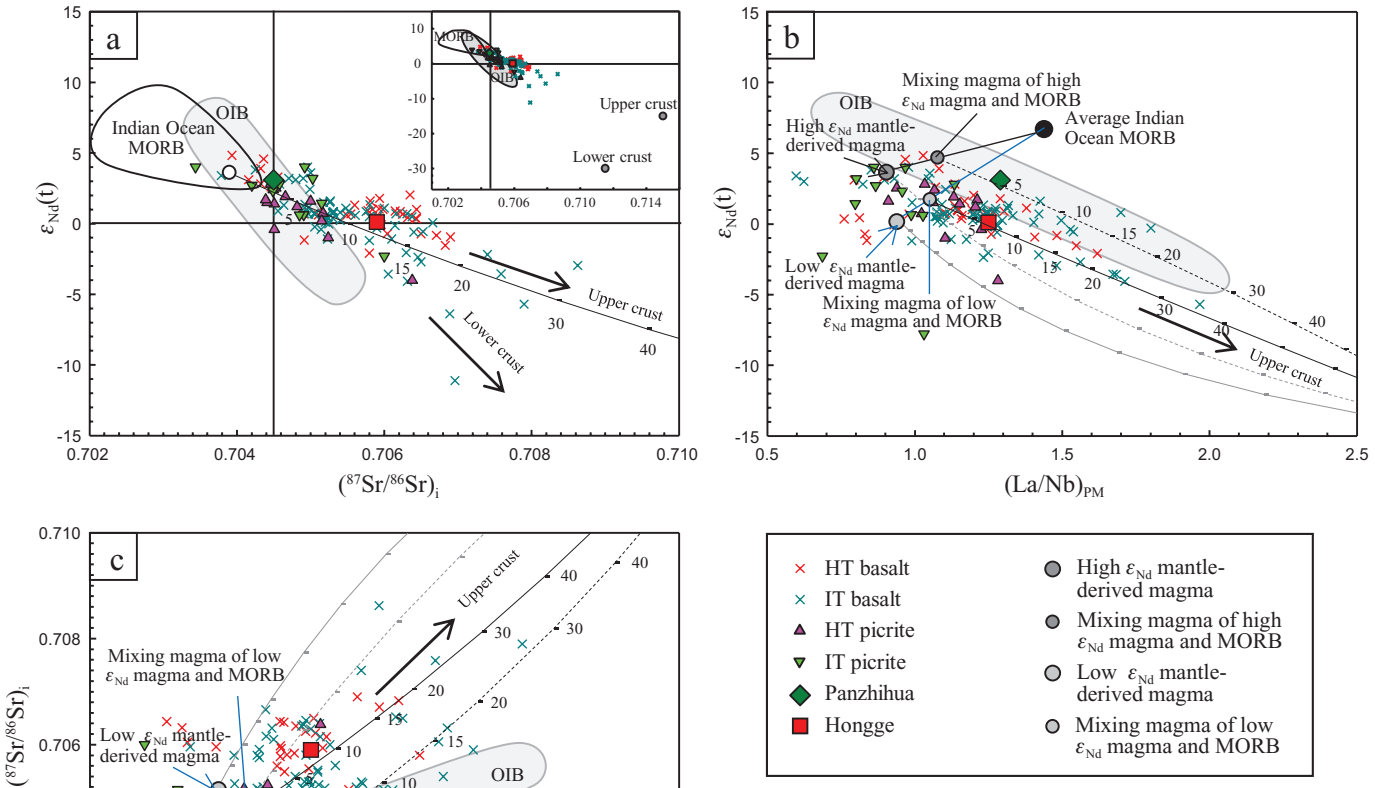

FIG. 14. Plots of $\varepsilon_{Nd(total)}$ values versus initial $^{87}Sr/^{86}Sr$ (a), $\varepsilon_{Nd(total)}$ values vs.s $(La/Nb)_{pm}$ (b) and initial $^{87}Sr/^{86}Sr$ vs. $(La/Nb)_{pm}$ (c) for the Hongge and Panzhihua intrusions and the Emeishan picrites and basalts. The OIB data are from the PetDB database (http://www.petdb.org). The average Indian Ocean MORB values are from Mahoney et al. (1998). The data for the lower and upper crusts are from Gao et al. (1999a, b), Chen and Jahn (1998), and Ma et al. (2000). The Emeishan picrites and basalts are from the GEOROC database (http://georoc.mpch-mainz.gwdg.de/georoc). The isotopic data for the Hongge and Panzhihua intrusions are from Zhong et al. (2003), Zhou et al. (2008), Zhang et al. (2009), and Pang et al. (2013).

melting, different sources, or melting at different depth (Xu et al., 2001, 2004; Xiao et al., 2004; Zhang et al., 2006, 2008; Hanski et al., 2010; He et al., 2010; Li et al., 2010).

The TiO_2 contents of most ocean island basalts are too high to be generated from a peridotite source mantle alone (Prytulak and Elliot, 2007). Hence, many researchers have suggested that the melting of ancient recycled old oceanic crust (i.e., eclogite) in the Emeishan mantle plume played a critical role in the generation of the high Ti basalts in the region (He et al., 2010; Hou et al., 2011b; Zhong et al., 2011; Kamenetsky et al., 2012). However, the $\delta^{18}O$ values for the majority of the Panzhihua clinopyroxene (3.9–5.4‰; Zhang et al., 2009) are significantly lower than those crystallized from normal mantle-derived magma (5.3–5.9‰; Ionov et al., 1994; Mattey et al., 1994; Chazot et al., 1997). Since the low $\delta^{18}O$ signature of altered oceanic crust cannot be preserved in the mantle for a long time, a more plausible explanation for low $\delta^{18}O$ values for the Panzhihua clinopyroxene crystals is the assimilation of high-temperature, altered, newly subducted oceanic gabbros by plume-derived magma during magma ascent. Based on different Sr-Nd isotopes and trace element ratios, we propose a new model involving variable inputs from the newly subducted, stagnant oxide-bearing gabbroic slab. As shown in Figure 1, the Hongge and Panzhihua intrusions occur at the western margin of the Yangtze block. The Tethyan oceanic plate was subducted eastward beneath the Yangtze block from the late Carboniferous to the Late Permian (Deng et al., 2013; Wang and Zhou, 2013). At ~260 Ma, the ascending Emeishan plume impinged on the newly subducted, stagnant oceanic lithospheric slab, which is similar to the relationship between the Yellowstone mantle plume and the Farallon-Juan de Fuca slab (Geist and Richards, 1993; Pierce et al., 2002; Xue and Allen, 2007; Coble and Mahood, 2012). When the ascending mantle plume-derived, picritic magma reached the overlying, newly subducted oceanic gabbros, Fe-Ti oxides in the gabbros would be preferentially dissolved into the magma because they were not saturated in the plume-derived magma. As this process continued, the ascending picritic magma became more enriched in TiO_2 and $FeO_{(total)}$.

Experiments have revealed that high Ti lunar basalts could have been produced by selective assimilation of Fe-Ti oxides from high Ti cumulates in the lunar crust by ascending primitive low Ti lunar basaltic magma from depth (Wagner and Grove, 1995, 1997; Elkins et al., 2000; Liang and Hess, 2006; van Kan Parker et al., 2011; Dygert et al., 2013). Figure 14a and b illustrate the conceptual mixing lines between mantle-derived magmas with different ε_{Nd} values within the ranges of the Emeishan picrites and the newly subducted oceanic gabbros with bulk isotope compositions and trace element ratios represented by the average Indian Ocean MORB (Mahoney et al., 1998). The estimated parental magma for the Panzhihua intrusion can be explained by mixing between mantle-derived magma with ε_{Nd} value close to the high end of the Emeishan picrites and the average MORB, followed by ~5 wt % contamination with the upper crust. The estimated parental magma for the Hongge intrusion can be explained by mixing between mantle-derived magma with ε_{Nd} value close to the low end of the Emeishan picrites and the average MORB, followed by ~5 wt % contamination with the upper crust. In either case the amounts of selective assimilation of oceanic oxide-bearing gabbros from the stagnant slab cannot be quantified because the abundance of trace elements in the assimilated phases is unknown.

It is intriguing that in the Emeishan large igneous province abundant world-class Fe-Ti oxide deposits are associated with more primitive magmas than elsewhere in the world. We believe that this is due to selective assimilation of newly subducted, stagnant oceanic lithospheric slab by the Emeishan plume-derived magma during magma ascent. This can be tested in the future by integrated isotope and trace element studies.

Conclusions

Important conclusions from this study are summarized below.

1. The accumulation of ilmenite and titanomagnetite in the base of clinopyroxenite layers and abundant oxide inclusions in olivine and clinopyroxene crystals in the Hongge magmatic Fe-Ti-V oxide deposit indicate high Ti content (>3.5 wt % TiO_2) in the parental magma for the deposit.

2. The accumulation of titanomagnetite in the base of gabbroic layers and abundant oxide inclusions in olivine and clinopyroxene crystals in the Panzhihua magmatic Fe-Ti-V oxide deposit indicate that the parental magma for this deposit contains lower TiO_2 than that of the Hongge deposit. This is also supported by higher TiO_2 in clinopyroxene with similar Mg numbers from the Hongge deposit than from the Panzhihua deposit.

3. Based on the compositions of clinopyroxene from the oxide ore-bearing lithologic units (zones), the estimated parental magma for the Honnge deposit has higher MgO/FeO and more fractionated mantle-normalized trace element patterns than that for the Panzhihua deposit.

4. The estimated parental magma compositions for the Hongge and Panzhihua deposits are similar to the average compositions of coeval Longzhoushan-type high Ti basalts and Ertan-type intermediate Ti basalts in the Permian Emeishan large igneous province, respectively.

5. The new trace element data, together with available Sr-Nd isotope data from the literature, indicate that interaction of mantle plume-derived magma with newly subducted, stagnant oceanic slab above the deep-seated Emeishn mantle plume and subsequent contamination with the upper crust all contributed to the compositional variations of the parental magmas for the Hongge and Panzhihua deposits.

6. More abundant Fe-Ti oxide ore deposits associated with less evolved basaltic magma in the Emeishan large igneous province than elsewhere in the world are attributed to selective assimilation of newly subducted oceanic lithospheric slab material by the ascending picritic magma derived from the deep-seated Emeishan mantle plume.

Acknowledgments

We thank Qian Mao in the State Key Laboratory of Lithospheric Evolution and Wen-Lan Zhang in the State Key Laboratory for Mineral Deposits Research for their assistance in EMPA. Sarah Dare, an anonymous reviewer, Larry Meinert, and Steve Barnes are thanked for their constructive reviews of this manuscript. This study was jointly supported by the

CAS/SAFEA International Partnership Program for Creative Research Teams-(Intraplate Mineralization Research Team; KZZD-EW-TZ-20), 12th Five-Year Plan project of SKLODG (SKLOG-ZY125-06; SKLODG-201202), the National Natural Science Foundation of China (41203040, 40873028), and Guizhou Provincial Natural Science Foundation (2294 of Y2013).

REFERENCES

Bai, Z.J., Zhong, H., Li, C., Zhu, W.G., and Xu, G.W., 2012a, Platinum-group elements in the oxide layers of the Hongge mafic-ultramafic intrusion, Emeishan large igneous province, SW China: Ore Geology Reviews, v. 46, p. 149–161.

Bai, Z.J., Zhong, H., Naldrett, A.J., Zhu, W.G., and Xu, G.W., 2012b, Whole-rock and mineral composition constraints on the genesis of the giant Hongge Fe-Ti-V oxide deposit in the Emeishan large igneous province, southwest China: Economic Geology, v. 107, p. 507–524.

Barnes, S.J., 1986, The effect of trapped liquid crystallization on cumulus mineral compositions in layered intrusions: Contributions to Mineralogy and Petrology, v. 93, p. 524–531.

Bédard, J.H., 2010, Parameterization of the Fe = Mg exchange coefficient (Kd) between clinopyroxene and silicate melts: Chemical Geology, v. 274, p. 169–176.

Botcharnikov, R.E., Almeev, R.R., Koepke, J., and Holtz, F., 2008, Phase relations and liquid lines of descent in hydrous ferrobasalt—implications for the Skaergaard intrusion and Columbia river flood basalts: Journal of Petrology, v. 49, p. 1687–1727.

Campbell, I.H., and Borley, G.D., 1974, The geochemistry of pyroxenes from the lower layered series of the Jimberlana intrusion, Western Australia: Contributions to Mineralogy and Petrology, v. 47, p. 281–297.

Cawthorn, R.G., 2013, Rare earth element abundances in apatite in the Bushveld Complex—a consequence of the trapped liquid shift effect: Geology, v. 41, p. 603–606.

Cawthorn, R.G., and Biggar, G.M., 1993, Crystallization of titaniferous chromite, magnesian ilmenite and armalcolite in tholeiitic suites in the Karoo igneous province: Contributions to Mineralogy and Petrology, v. 114, p. 221–235.

Cawthorn, R.G., Groves, D.I., and Marchant, T., 1985, Magnesian ilmenite: Clue to high-Mg parental magma of the Insizwa Complex, Transkei: Canadian Mineralogist, v. 23, p. 609–618.

Cawthorn, R.G., Bristow, J.W., and Groves, D.I., 1989, Magnesian ilmenite in picritic basalts from the Karoo Province, South-Africa: Mineralogical Magazine, v. 53, p. 245–252.

Chazot, G., Lowry, D., Menzies, and M., Mattey, D., 1997, Oxygen isotopic composition of hydrous and anhydrous mantle peridotites: Geochimica et Cosmochimica Acta, v. 61, p. 161–169.

Chen, J.F., and Jahn, B.M., 1998, Crustal evolution of southeastern China: Nd and Sr isotopic evidence: Tectonophysics, v. 284, p. 101–133.

Cherniak, D.J., and Liang, Y., 2012, Ti diffusion in natural pyroxene: Geochimica et Cosmochimica Acta, v. 98, p. 31–47.

Coble, M.A., and Mahood, G.A., 2012, Initial impingement of the Yellowstone plume located by widespread silicic volcanism contemporaneous with Columbia River flood basalts: Geology, v. 40, p. 655–658.

Chung, S.L., and Jahn, B.M., 1995, Plume-lithosphere interaction in generation of the Emeishan flood basalts at the Permian-Triassic boundary: Geology, v. 23, p. 889–892.

Deng, J., Wang, Q., Li, G., Li, C., and Wang, C., 2013, Tethys tectonic evolution and its bearing on the distribution of important mineral deposits in the Sanjiang region, SW China: Gondwana Research, doi: 10.1016/j.gr.2013.08.002.

Dong, H., Xing, C., and Wang, C.Y., 2013, Textures and mineral compositions of the Xinjie layered intrusion, SW China: Implications for the origin of magnetite and fractionation process of Fe-Ti-rich basaltic magmas: Geoscience Frontiers, v. 4, p. 503–515.

Dygert, N., Liang, Y., and Hess, P., 2013, The importance of melt TiO_2 in affecting major and trace element partitioning between Fe-Ti oxides and lunar picritic glass melts: Geochimica et Cosmochimica Acta, v. 106, p. 134–151.

Elkins, L.T., Fernandes, V.A., Delano, J.W., and Grove, T.L., 2000, Origin of lunar ultramafic green glasses: Constraints from phase equilibrium studies: Geochimica et Cosmochimica Acta, v. 64, p. 2339–2350.

Fan, W.M., Wang, Y.J., Peng, T.P., Miao, L.C., and Guo, F., 2004, Ar-Ar and U-Pb geochronol- ogy of late Paleozoic basalts in western Guangxi and its constraints on the eruption age of Emeishan basalt magmatism: Chinese Science Bulletin, v. 49, p. 2318–2327.

Fan, W.M., Zhang, C.H., Wang, Y.J., Guo, F., and Peng, T.P., 2008, Geochronology and geochemistry of Permian basalts in western Guangxi Province, southwest China: Evidence for plume-lithosphere interaction: Lithos, v. 102, p. 218–236.

Gaetani, G., Kent, A.R., Grove, T., Hutcheon, I., and Stolper, E., 2003, Mineral/melt partitioning of trace elements during hydrous peridotite partial melting: Contributions to Mineralogy and Petrology, v. 145, p. 391–405.

Ganino, C., Arndt, N.T., Zhou, M.F., Gaillard, F., and Chauvel, C., 2008, Interaction of magma with sedimentary wall rock and magnetite ore genesis in the Panzhihua mafic intrusion, SW China: Mineralium Deposita, v. 43, p. 677–694.

Gao, S., Lin, W.L., and Qiu, Y.M., 1999a, Contrasting geochemical and Sm-Nd isotopic compositions of Archaean metasediments from the Kongling high-grade terrain of the Yangtze craton: Evidence for cratonic evolution and redistribution of REE during crustal anatexis: Geochimica et Cosmochimica Acta, p. 63, p. 2071–2088.

Gao, S., Luo, T.C., Zhang, B.R., Zhang, H.F., Han, Y.W., Zhao, Z.D., and Hartmut, K., 1999b, Structure and composition of the continental crust in East China: Science China Earth Sciences, v. 42, p. 129–140.

Geist, D., and Richards, M., 1993, Origin of the Columbia Plateau and Snake River plain: Deflection of the Yellowstone plume: Geology, v. 21, p. 789–792.

Godel, B., Barnes, S.-J., and Maier, W.D., 2011, Parental magma composition inferred from trace element in cumulus and intercumulus silicate minerals: An example from the Lower and Lower Critical zones of the Bushveld Complex, South-Africa: Lithos, v. 125, p. 537–552.

Hanski, E., Kamenetsky, V.S., Luo, Z.Y., Xu, Y.G., and Kuzmin, D.V., 2010, Primitive magmas in the Emeishan large igneous province, southwestern China and northern Vietnam: Lithos, v. 119, p. 75–90.

Hart, S.R., and Dunn, T., 1993, Experimental cpx/melt partitioning of 24 trace elements: Contributions to Mineralogy and Petrology, v. 113, p. 1–8.

Hauri, E.H., Wagner, T.P., and Grove, T.L., 1994, Experimental and natural partitioning of Th, U, Pb and other trace elements between garnet, clinopyroxene and basaltic melts: Chemical Geology, v. 117, p. 149–166.

He, Q., Xiao, L., Balta, B., Gao, R., and Chen, J., 2010, Variety and complexity of the Late-Permian Emeishan basalts: Reappraisal of plume-lithosphere interaction processes: Lithos, v. 119, p. 91–107.

Hill, E., Wood, B.J., and Blundy, J.D., 2000, The effect of Ca-Tschermaks component on trace element partitioning between clinopyroxene and silicate melt: Lithos, v. 53, p. 203–215.

Hou, T., Zhang, Z.C., Kusky, T., Du, Y.S., Liu, J.L., and Zhao, Z.D., 2011a, A reappraisal of the high-Ti and low-Ti classification of basalts and petrogenetic linkage between basalts and mafic-ultramafic intrusions in the Emeishan large igneous province, SW China: Ore Geology Reviews, v. 41, p. 133–143.

Hou, T., Zhang, Z., Ye, X., Encarnacion, J., and Reichow, M.K., 2011b, Noble gas isotopic systematics of Fe-Ti-V oxide ore-related mafic-ultramafic layered intrusions in the Panxi area, China: The role of recycled oceanic crust in their petrogenesis: Geochimica et Cosmochimica Acta, v. 75, p. 6727–6741.

Hou, T., Zhang, Z.C., and Pirajno, F., 2012, A new metallogenic model of the Panzhihua giant V-Ti-iron oxide deposit (Emeishan large igneous province) based on high-Mg olivine-bearing wehrlite and new field evidence: International Geology Review, v. 54, p. 1721–1745.

Howarth, G.H., and Prevec, S.A., 2013a, Trace element, PGE, and Sr-Nd isotope geochemistry of the Panzhihua mafic layered intrusion, SW China: Constraints on ore-forming processes and evolution of parent magma at depth in a plumbing-system: Geochimica et Cosmochimica Acta, v. 120, p. 459–478.

——2013b, Hydration vs. oxidation: Modelling implications for Fe-Ti oxide crystallisation in mafic intrusions, with specific reference to the Panzhihua intrusion, SW China: Geoscience Frontiers, v. 4, p. 555–569.

Hu, Z.C., Gao, S., Liu, Y.S., Hu, S.H., Chen, H.H., and Yuan, H.L., 2008, Signal enhancement in laser ablation ICP-MS by addition of nitrogen in the central channel gas: Journal of Analytical Atomic Spectrometry, v. 23, p. 1093–1101.

Ionov, D.A., Harmon, R.S., France-Lanord, C., Greenwood, P.B., and Ashchepkov, I.V., 1994, Oxygen isotope composition of garnet and spinel peridotites in the continental mantle: Evidence from the Vitim xenolith suite, southern Siberia: Geochimica et Cosmochimica Acta, v. 58, p. 1463–1470.

Irvine, T., 1970, Crystallization sequences in the Muskox intrusion and other layered intrusions. I. Olivine-pyroxene-plagioclase relations: Geological Society of South Africa Special Publication 1, p. 441–476.

Jugo, P.J., Luth, R.W., and Richards, J.P., 2005, Experimental data on the speciation of sulfur as a function of oxygen fugacity in basaltic melts: Geochimica et Cosmochimica Acta, v. 69, p. 497–503.

Kamenetsky, V.S., Chung, S.L., Kamenetsky, M.B., and Kuzmin, D.V., 2012, Picrites from the Emeishan large igneous province, SW China: A compositional continuum in primitive magmas and their respective mantle sources: Journal of Petrology, v. 53, p. 2095–2113.

Lai, S.C., Qin, J.F., Li, Y.F., Li, S.Z., and Santosh, M., 2012, Permian high Ti/Y basalts from the eastern part of the Emeishan large igneous province, southwestern China: Petrogenesis and tectonic implications: Journal of Asian Earth Sciences, v. 47, p. 216–230.

Li, C., Tao, Y., Qi, L., and Ripley, E.M., 2012, Controls on PGE fractionation in the Emeishan picrites and basalts: Constraints from integrated lithophile-siderophile elements and Sr-Nd isotopes: Geochimica et Cosmochimica Acta, v. 90, p. 12–32.

Li, J., Xu, J.F., Suzuki, K., He, B., Xu, Y.G., and Ren, Z.Y., 2010, Os, Nd and Sr isotope and trace element geochemistry of the Muli picrites: Insights into the mantle source of the Emeishan large igneous province: Lithos, v. 119, p. 108–122.

Li, X.H., Li, Z.X., Sinclair, J.A., Li, W.X., and Carter, G., 2006, Revisiting the "Yanbian Terrane:" Implications for Neoproterozoic tectonic evolution of the western Yangtze block, south China: Precambrian Research, v. 151, p. 14–30.

Li, Z.X., Li, X.H., Kinny, P.D., Wang, J., Zhang, S., and Zhou, H., 2003, Geochronology of Neoproterozoic syn-rift magmatism in the Yangtze craton, south China and correlations with other continents: Evidence for a mantle superplume that broke up Rodinia: Precambrian Research, v. 122, p. 85–109.

Liang, Y., and Hess, P., 2006. Preferential assimilation due to melt-rock reaction in the Lunar mantle: A laboratory and ophiolite field perspective [abs.]: Annual Lunar and Planetary Science Conference, 37th, Abstracts, p. 1943.

Liu, D., Shen, F.K., and Zhang, G.Z., 1985, Layered intrusions of the Panxi area, Sichuan province, *in* Zhang, Y.X., ed., Corpus of the Panxi paleorift studies in China: Geological Press, p. 85–118 (in Chinese).

Liu, Y.S., Hu, Z.C., Gao, S., Günther, D., Xu, J., Gao, C.G., and Chen, H.H., 2008, In situ analysis of major and trace elements of anhydrous minerals by LA-ICP-MS without applying an internal standard: Chemical Geology, v. 257, p. 34–43.

Liu, Y.S., Gao, S., Hu, Z.C., Gao, C.G., Zong, K.Q., and Wang, D.B., 2010, Continental and oceanic crust recycling-induced melt-peridotite interactions in the Trans-North China orogen: U-Pb dating, Hf isotopes and trace elements in zircons of mantle xenoliths: Journal of Petrology, v. 51, p. 537–571.

Luan, Y., Song, X.Y., Chen, L.M., Zheng, W.Q., Zhang, X.Q., Yu, S.Y., She, Y.W., Tian, X.L., and Ran, Q.Y., 2014, Key factors controlling the accumulation of the Fe-Ti oxides in the Hongge layered intrusion in the Emeishan large igneous province, SW China: Ore Geology Reviews, v. 57, p. 518–538.

Lundstrom, C.C., Shaw, H.F., Ryerson, F.J., Williams, Q., and Gill, J., 1998, Crystal chemical control of clinopyroxene-melt partitioning in the Di-Ab-An system: Implications for elemental fractionations in the depleted mantle: Geochimica et Cosmochimica Acta, v. 62, p. 2849–2862.

Ma, C.Q., Ehlers, C., and Xu, C.H., 2000, The roots of the Dabieshan ultrahigh-pressure metamorphic terrain: Constraints from geochemistry and Nd-Sr isotope systematics: Precambrian Research, v. 102, p. 279–301.

Ma, Y., Ji, X.T., Li, J.C., Huang, M., and Kan, Z.Z., 2003, Mineral resources of the Panzhihua region: Chengdu, Sichuan Science and Technology Press, 275 p. (in Chinese).

Mahoney, J.J., Frei, R., Tejad, M.L.G., Mo, X.X., Leat, P.T., and Nägler, T.F., 1998, Tracing the Indian Ocean mantle domain through time: Isotopic results from old West Indian, East Tethyan, and South Pacific seafloor: Journal of Petrology, v. 39, p. 1285–1306.

Mattey, D., Lowry, D., and Macpherson, C., 1994, Oxygen isotope composition of mantle peridotite: Earth and Planetary Science Letters, v. 128, p. 231–241.

McBirney, A.R., 1989, The Skaergaard layered series: I. Structure and average compositions: Journal of Petrology, v. 30, p. 363–397.

——1996, The Skaergaard intrusion, *in* Cawthorn, R.G., ed., Layered intrusions: Elsevier, p. 147–180.

McCarthy, T.S., and Cawthorn, R.G., 1983, The geochemistry of vanadiferous magnetite in the Bushveld complex: Implications for crystallization mechanisms in layered complexes: Mineralium Deposita, v. 18, p. 505–518.

Murari, R., Krishnamurthy, P., Tikhonenko, P., and Gopalan, K., 1993, Magnesian ilmenites in picrite basalts from Siberian and Deccan traps: Additional mineralogical evidence for primary melt compositions (?): Mineralogical Magazine, v. 57, p. 733–735.

Nielsen, R.L., and Beard, J.S., 2000, Magnetite-melt HFSE partitioning: Chemical Geology, v. 164, p. 21–34.

Pang, K.N., 2008, Origin of the Permian Panzhihua layered gabbroic intrusion and the hosted Fe-Ti-V oxide deposits, Sichuan Province, SW China: Unpublished Ph.D. thesis, Hong Kong, University of Hong Kong.

Pang, K.N., Li, C., Zhou, M.F., and Ripley, E., 2008a, Abundant Fe-Ti oxide inclusions in olivine from the Panzhihua and Hongge layered intrusions, SW China: Evidence for early saturation of Fe-Ti oxides in ferrobasaltic magma: Contributions to Mineralogy and Petrology, v. 156, p. 307–321.

Pang, K.N., Zhou, M.F., Lindsley, D., Zhao, D.G., and Malpas, J., 2008b, Origin of Fe-Ti oxide ores in mafic intrusions: Evidence from the Panzhihua intrusion, SW China: Journal of Petrology, v. 49, p. 295–313.

Pang, K.N., Li, C., Zhou, M.F., and Ripley, E.M., 2009, Mineral compositional constraints on petrogenesis and oxide ore genesis of the late Permian Panzhihua layered gabbroic intrusion, SW China: Lithos, v. 110, p. 199–214.

Pang, K.N., Zhou, M.F., Qi, L., Shellnutt, G., Wang, C.Y., and Zhao, D., 2010, Flood basalt-related Fe-Ti oxide deposits in the Emeishan large igneous province, SW China: Lithos, v. 119, p. 123–136.

Pang, K.N., Zhou, M.F., Qi, L., Chung, S.L., Chu, C.H., and Lee, H.Y., 2013, Petrology and geochemistry at the Lower zone-Middle zone transition of the Panzhihua intrusion, SW China: Implications for differentiation and oxide ore genesis: Geoscience Frontiers, v. 4, p. 517–533.

Pierce, K.L., Morgan, L.A., and Saltus, R.W., 2002, Yellowstone plume head: Postulated tectonic relations to the Vancouver slab, continental boundaries, and climate: Idaho Geological Survey Bulletin, v. 30, p. 5–33.

Prytulak, J., and Elliott, T., 2007, TiO_2 enrichment in ocean island basalts: Earth and Planetary Science Letters, v. 263, p. 388–403.

PXGT (Pan-Xi Geological Team), 1987, Metallogenetic conditions and geologic characters of the Hongge vanadic titanomagnetite deposit, Sichuan: Beijing, Geological Publishing House, 220 p. (in Chinese).

Qi, L., Wang, C.Y., and Zhou, M.F., 2008, Controls on the PGE distribution of Permian Emeishan alkaline and peralkaline volcanic rocks in Longzhoushan, Sichuan Province, SW China: Lithos, v. 106, p. 222–236.

Rollinson, H.R., 1993, Using geochemical data: Evaluation, presentation, interpretation: New York, Longman Scientific and Technical, 108 p.

Shellnutt, J., and Pang, K.N., 2012, Petrogenetic implications of mineral chemical data for the Permian Baima igneous complex, SW China: Mineralogy and Petrology, v. 106, p. 75–88.

Snyder, D., Carmichael, I.S.E., and Wiebe, R.A., 1993, Experimental study of liquid evolution in an Fe-rich, layered mafic intrusion: Constraints of Fe-Ti oxide precipitation on the T-f_{O_2} and T-ϱ paths of tholeiitic magmas: Contributions to Mineralogy and Petrology, v. 113, p. 73–86.

Song, X.Y., Qi, H.W., Robinson, P.T., Zhou, M.F., Cao, Z.M., and Chen, L.M., 2008, Melting of the subcontinental lithospheric mantle by the Emeishan mantle plume: Evidence from the basal alkaline basalts in Dongchuan, Yunnan, southwestern China: Lithos, v. 100, p. 93–111.

Song, X.Y., Qi, H.W., Hu, R.Z., Chen, L.M., Yu, S.Y., and Zhang, J.F., 2013, Formation of thick stratiform Fe-Ti oxide layers in layered intrusion and frequent replenishment of fractionated mafic magma: Evidence from the Panzhihua intrusion, SW China: Geochemistry, Geophysics, Geosystems, v. 14, p. 712–732.

Sparks, R.S.J., 1986, The role of crustal contamination in magma evolution through geological time: Earth and Planetary Science Letters, v. 78, p. 211–223.

Sun, S.S., and McDonough, W.F., 1989, Chemical and isotopic systematics of oceanic basalts: Implications for mantle composition and processes, *in* Saunders, A.D., and Norry, M.J., eds., Magmatism in the ocean basins: Geological Society London Special Publications, p. 313–345.

Tegner, C., Cawthorn, R.G., and Kruger, F.J., 2006, Cyclicity in the Main and Upper zones of the Bushveld Complex, South Africa: Crystallization from a zoned magma sheet: Journal of Petrology, v. 47, p. 2257–2279.

Tegner, C., Thy, P., Holness, M.B., Jakobsen, J.K., and Lesher, C.E., 2009, Differentiation and compaction in the Skaergaard iIntrusion: Journal of Petrology, v. 50, p. 813–840.

Thy, P., Lesher, C.E., and Tegner, C., 2009, The Skaergaard liquid line of descent revisited: Contributions to Mineralogy and Petrology, v. 157, p. 735–747.

Toplis, M.J., and Carroll, M.R., 1995, An experimental study of the influence of oxygen fugacity on Fe-Ti oxide stability, phase relations, and mineral-melt equilibria in ferro-basaltic systems: Journal of Petrology, v. 36, p. 1137–1170.

van Kan Parker, M., Mason, P.R.D., and van Westrenen, W., 2011, Trace element partitioning between ilmenite, armalcolite and anhydrous silicate melt: Implications for the formation of lunar high-Ti mare basalts: Geochimica et Cosmochimica Acta, v. 75, p. 4179–4193.

Wagner, T., and Grove, T., 1995, Origin of high-Ti lunar magma by erosion of ilmenite [abs.]: Lunar and Planetary Institute Science Conference Abstracts, p. 1455.

——1997, Experimental constraints on the origin of lunar high-Ti ultramafic glasses: Geochimica et Cosmochimica Acta, v. 61, p. 1315–1327.

Wang, C., Deng, J., Carranza, E.J.M., and Santosh, M., 2013, Tin metallogenesis associated with granitoids in the southwestern Sanjiang Tethyan domain: Nature, deposit types, and tectonic setting: Gondwana Research, doi: 10.1016/j.gr.2013.05.005.

Wang, C.Y., and Zhou, M.F., 2013, New textural and mineralogical constraints on the origin of the Hongge Fe-Ti-V oxide deposit, SW China: Mineralium Deposita, v. 48, p. 787–798.

Wang, C.Y., Zhou, M.F., and Qi, L., 2007, Permian flood basalts and mafic intrusions in the Jinping (SW China)-Song Da (northern Vietnam) district: Mantle sources, crustal contamination and sulfide segregation: Chemical Geology, v. 243, p. 317–343.

Wang, C.Y., Zhou, M.-F., and Zhao, D., 2008, Fe-Ti-Cr oxides from the Permian Xinjie mafic-ultramafic layered intrusion in the Emeishan large igneous province, SW China: Crystallization from Fe- and Ti-rich basaltic magmas: Lithos, v. 102, p. 198–217.

Xiao, L., Xu, Y.G., Mei, H.J., Zheng, Y.F., He, B., and Pirajno, F., 2004, Distinct mantle sources of low-Ti and high-Ti basalts from the western Emeishan large igneous province, SW China: Implications for plume-lithosphere interaction: Earth and Planetary Science Letters, v. 228, p. 525–546.

Xu, J.F., Suzuki, K., Xu, Y.G., Mei, H.J., and Li, J., 2007, Os, Pb, and Nd isotope geochemistry of the Permian Emeishan continental flood basalts: Insights into the source of a large igneous province: Geochimica et Cosmochimica Acta, v. 71, p. 2104–2119.

Xu, Y.G., Chung, S.L., Jahn, B.M., and Wu, G.Y., 2001, Petrologic and geochemical constraints on the petrogenesis of Permian-Triassic Emeishan flood basalts in southwestern China: Lithos, v. 58, p. 145–168.

Xue, M., and Allen, R.M., 2007, The fate of the Juan de Fuca plate: Implications for a Yellowstone plume head: Earth and Planetary Science Letters, v. 264, p. 266–276.

Yao, P.H., Wang, K.N., Du, C.L., Lin, Z.T., and Song, X., 1993, Records of China's iron ore deposits: Beijing, Metallurgical Industry Press (in Chinese).

Zhang, Z.C., Mahoney, J.J., Mao, J.W., and Wang, F.S., 2006, Geochemistry of picritic and associated basalt flows of the western Emeishan flood basalt province, China: Journal of Petrology, v. 47, p. 1997–2019.

Zhang, Z.C., Zhi, X.C., Chen, L., Saunders, A.D., and Reichow, M.K., 2008, Re-Os isotopic compositions of picrites from the Emeishan flood basalt province, China: Earth and Planetary Science Letters, v. 276, p. 30–39.

Zhang, Z.C., Mao, J.W., Saunders, A.D., Ai, Y., Li, Y., and Zhao, L., 2009, Petrogenetic modeling of three mafic-ultramafic layered intrusions in the Emeishan large igneous province, SW China, based on isotopic and bulk chemical constraints: Lithos, v. 113, p. 369–392.

Zhong, H., and Zhu, W.G., 2006, Geochronology of layered mafic intrusions from the Pan-Xi area in the Emeishan large igneous province, SW China: Mineralium Deposita, v. 41, p. 599–606.

Zhong, H., Zhou, X.H., Zhou, M.F., Sun, M., and Liu, B.G., 2002, Platinum-group element geochemistry of the Hongge Fe-V-Ti deposit in the Pan-Xi area, southwestern China: Mineralium Deposita, v. 37, p. 226–239.

Zhong, H., Yao, Y., Hu, S.F., Zhou, X.H., Liu, B.G., Sun, M., Zhou, M.F., and Viljoen, M.J., 2003, Trace-element and Sr-Nd isotopic geochemistry of the PGE-bearing Hongge layered intrusion, southwestern China: International Geology Review, v. 45, p. 371–382.

Zhong, H., Hu, R.Z., Wilson, A., and Zhu, W.G., 2005, Review of the link between the Hongge layered intrusion and Emeishan flood basalts, southwest China: International Geology Review, v. 47, p. 971–985.

Zhong, H., Qi, L., Hu, R.Z., Zhou, M.F., Gou, T.Z., Zhu, W.G., Liu, B.G., and Chu, Z.Y., 2011, Rhenium-osmium isotope and platinum-group elements in the Xinjie layered intrusion, SW China: Implications for source mantle composition, mantle evolution, PGE fractionation and mineralization: Geochimica et Cosmochimica Acta, v. 75, p. 1621–1641.

Zhou, M.F., Malpas, J., Song, X.Y., Robinson, P.T., Sun, M., Kennedy, A.K., Lesher, C.M., and Keays, R.R., 2002, A temporal link between the Emeishan large igneous province (SW China) and the end-Guadalupian mass extinction: Earth and Planetary Science Letters, v. 196, p. 113–122.

Zhou, M.F., Robinson, P.T., Lesher, C.M., Keays, R.R., Zhang, C.J., and Malpas, J., 2005, Geochemistry, petrogenesis and metallogenesis of the Panzhihua gabbroic layered intrusion and associated Fe-Ti-V oxide deposits, Sichuan province, SW China: Journal of Petrology, v. 46, p. 2253–2280.

Zhou, M.F., Ma, Y., Yan, D.P., Xia, X., Zhao, J.H., and Sun, M., 2006, The Yanbian terrane (southern Sichuan province, SW China): A Neoproterozoic arc assemblage in the western margin of the Yangtze block: Precambrian Research, v. 144, p. 19–38.

Zhou, M.F., Arndt, N.T., Malpas, J., Wang, C.Y., and Kennedy, A.K., 2008, Two magma series and associated ore deposit types in the Permian Emeishan large igneous province, SW China: Lithos, v. 103, p. 352–368.

Zhou, M.F., Chen, W.T., Wang, C.Y., Prevec, S.A., Liu, Patricia P., and Howarth, G.H., 2013, Two stages of immiscible liquid separation in the formation of Panzhihua-type Fe-Ti-V oxide deposits, SW China: Geoscience Frontiers, v. 4, p. 481–502.

Zhu, W.G., Zhong, H., Deng, H.L., Wilson, A.H., Liu, B.G., Li, C.Y., and Qin, Y., 2006, SHRIMP zircon U-Pb age, geochemistry, and Nd-Sr isotopes of the Gaojiacun mafic-ultramafic intrusive complex, southwest China: International Geology Review, v. 48, p. 650–668.